Forward production of Υ mesons in pp collisions at $\sqrt{s} = 7$ and 8 TeV

LHCb Collaboration ; Aaij, R ; Adeva, B ; Adinolfi, M ; Anderson, J ; Bernet, R ; Bowen, E ; Bursche, A ; Chiapolini, N ; Chrzaszcz, M ; Dey, B ; Elsasser, C ; Graverini, E ; Lionetto, F ; Lowdon, P ; Mauri, A ; Müller, K ; Serra, N ; Steinkamp, O ; Storaci, B ; Straumann, U ; Tresch, M ; Vollhardt, A ; Weiden, A ; et al

Abstract: The production of Υ mesons in pp collisions at $\sqrt{=}7$ and 8 TeV is studied with the LHCb detector using data samples corresponding to an integrated luminosity of $1\,\text{fb}^{-1}$ and $2\,\text{fb}^{-1}$ respectively. The production cross-sections and ratios of cross-sections are measured as functions of the meson transverse momentum p_T and rapidity y, for $p_T < 30\,\text{GeV}/c$ and $2.0 < y < 4.5$.

DOI: https://doi.org/10.1007/JHEP11(2015)103

Originally published at:
LHCb Collaboration; Aaij, R; Adeva, B; Adinolfi, M; Anderson, J; Bernet, R; Bowen, E; Bursche, A; Chiapolini, N; Chrzaszcz, M; Dey, B; Elsasser, C; Graverini, E; Lionetto, F; Lowdon, P; Mauri, A; Müller, K; Serra, N; Steinkamp, O; Storaci, B; Straumann, U; Tresch, M; Vollhardt, A; Weiden, A; et al (2015). Forward production of Υ mesons in pp collisions at $\sqrt{s} = 7$ and 8 TeV. Journal of High Energy Physics, 2015(11):103.
DOI: https://doi.org/10.1007/JHEP11(2015)103

EUROPEAN ORGANIZATION FOR NUCLEAR RESEARCH (CERN)

CERN-PH-EP-2015-232
LHCb-PAPER-2015-045
September 8, 2015

Forward production of Υ mesons in pp collisions at $\sqrt{s} = 7$ and 8 TeV

The LHCb collaboration[†]

Abstract

The production of Υ mesons in pp collisions at $\sqrt{s} = 7$ and 8 TeV is studied with the LHCb detector using data samples corresponding to an integrated luminosity of $1\,\text{fb}^{-1}$ and $2\,\text{fb}^{-1}$ respectively. The production cross-sections and ratios of cross-sections are measured as functions of the meson transverse momentum p_{T} and rapidity y, for $p_{\text{T}} < 30\,\text{GeV}/c$ and $2.0 < y < 4.5$.

Published in JHEP 1511(2015) 103

[†]Authors are listed at the end of this paper.

1 Introduction

In high energy hadron collisions, the production of heavy quarkonium systems such as the $b\bar{b}$ states ($\Upsilon(1S)$, $\Upsilon(2S)$ and $\Upsilon(3S)$, represented generically as Υ in the following) probes the dynamics of the colliding partons and provides insight into the non-perturbative regime of quantum chromodynamics (QCD). Despite many models that have been proposed, a complete description of heavy quarkonium production is still not available.

The effective theory of non-relativistic QCD (NRQCD) [1, 2] provides the foundation for much of the current theoretical work. According to NRQCD, the production of heavy quarkonium factorises into two steps: a heavy quark-antiquark pair is first created at short distances, and subsequently evolves non-perturbatively into a quarkonium state. The NRQCD calculations include the colour-singlet (CS) and colour-octet (CO) matrix elements for the pertubative stage. The CS model [3, 4], which provides a leading-order description of quarkonium production, underestimates the cross-section for single J/ψ production at the Tevatron [5] at high $p_{\rm T}$, where $p_{\rm T}$ is the component of the meson momentum transverse to the beam. To resolve this discrepancy, the CO mechanism was introduced [6]. The corresponding matrix elements were determined from the high-$p_{\rm T}$ data, as the CO cross-section decreases more slowly with $p_{\rm T}$ than that predicted by the CS model. More recent higher-order calculations [7–11] show better agreement between CS predictions and the experimental data [12], reducing the need for large CO contributions. The production of Υ mesons in proton-proton (pp) collisions can occur either directly in parton scattering or via feed down from the decay of heavier bottomonium states, such as $\chi_{\rm b}$ [13–18], or higher-mass Υ states, which complicates the theoretical description of bottomonium production [19, 20].

The production of the Υ mesons has been studied using pp collision data taken at $\sqrt{s} = 2.76$, 7 and 8 TeV by the LHCb [21–23], ALICE [24], ATLAS [25] and CMS [26, 27] experiments in different kinematic regions. The existing LHCb measurements of these quantities were performed at $\sqrt{s} = 7\,\text{TeV}$ with a data sample collected in 2010 corresponding to an integrated luminosity of $25\,\text{pb}^{-1}$, and at $\sqrt{s} = 8\,\text{TeV}$ for early 2012 data using $50\,\text{pb}^{-1}$. Both measurements were differential in $p_{\rm T}$ and y of the Υ mesons in the ranges $2.0 < y < 4.5$ and $p_{\rm T} < 15\,\text{GeV}/c$. Based on these measurements, an increase of the production cross-section in excess of 30% between $\sqrt{s} = 7$ and 8 TeV was observed, which is larger than the increase observed for other quarkonium states such as the J/ψ [23, 28] and larger than the expectations from NRQCD [11].

In this paper we report on the measurement of the inclusive production cross-sections of the Υ states at $\sqrt{s} = 7$ and 8 TeV and the ratios of these cross-sections. The Υ cross-section measurement is performed using a data sample corresponding to the complete LHCb Run 1 data set with integrated luminosities of $1\,\text{fb}^{-1}$ and $2\,\text{fb}^{-1}$, accumulated at $\sqrt{s} = 7$ and 8 TeV, respectively. These samples are independent from those used in the previous analyses [22,23]. The increased size of the data sample results in a better statistical precision and allows the measurements to be extended up to $p_{\rm T}$ values of $30\,\text{GeV}/c$.

2 Detector and simulation

The LHCb detector [29,30] is a single-arm forward spectrometer covering the pseudorapidity range $2 < \eta < 5$, designed for the study of particles containing b or c quarks. The detector includes a high-precision tracking system consisting of a silicon-strip vertex detector surrounding the pp interaction region, a large-area silicon-strip detector located upstream of a dipole magnet with a bending power of about 4 Tm, and three stations of silicon-strip detectors and straw drift tubes placed downstream of the magnet. The tracking system provides a measurement of momentum, p, of charged particles with a relative uncertainty that varies from 0.5% at low momentum to 1.0% at 200 GeV/c. The minimum distance of a track to a primary vertex, the impact parameter, is measured with a resolution of $(15 + 29/p_{\rm T})$ μm, where $p_{\rm T}$ is in GeV/c. Different types of charged hadrons are distinguished using information from two ring-imaging Cherenkov detectors. Photons, electrons and hadrons are identified by a calorimeter system consisting of scintillating-pad and preshower detectors, an electromagnetic calorimeter and a hadronic calorimeter. Muons are identified by a system composed of alternating layers of iron and multiwire proportional chambers [31]. The online event selection is performed by a trigger [32], which consists of a hardware stage, based on information from the calorimeter and muon systems, followed by a software stage, which applies a full event reconstruction. At the hardware stage, events for this analysis are selected by requiring dimuon candidates with a product of their $p_{\rm T}$ values exceeding 1.7 (2.6) (GeV/c)^2 for data collected at $\sqrt{s} = 7$ (8) TeV. In the subsequent software trigger, two well-reconstructed tracks are required to have hits in the muon system, $p_{\rm T} > 500$ MeV/c, $p > 6$ GeV/c and to form a common vertex. Only events with a dimuon candidate with a mass $m_{\mu^+\mu^-} > 4.7$ GeV/c^2 are retained for further analysis. In the offline selection, trigger decisions are associated with reconstructed particles. Selection requirements can therefore be made on the trigger selection itself and on whether the decision was due to the signal candidate, the other particles produced in the pp collision, or a combination of both.

In the simulation, pp collisions are generated using Pythia 6 [33] with a specific LHCb configuration [34]. Decays of hadronic particles are described by EvtGen [35], in which final-state radiation is generated using Photos [36]. The interaction of the generated particles with the detector, and its response, are implemented using the Geant4 toolkit [37] as described in Ref. [38].

3 Selection and cross-section determination

The event selection is based on the criteria described in the previous LHCb Υ analyses [21–23] but slightly modified to improve the signal-to-background ratio. It includes selection criteria that ensure good quality track reconstruction [39], muon identification [40], and the requirement of a good fit quality for the dimuon vertex, where the associated primary vertex position is used as a constraint in the fit [41]. In addition, the muon candidates are required to have $1 < p_{\rm T} < 25$ GeV/c, $10 < p < 400$ GeV/c and pseudorapidity within the region $2.0 < \eta < 4.5$.

The differential cross-section for the production of an Υ meson decaying into a muon pair is

$$\mathcal{B}_\Upsilon \times \frac{\mathrm{d}^2}{\mathrm{d}p_\mathrm{T}\,\mathrm{d}y}\sigma(\mathrm{pp}\to\Upsilon\mathrm{X}) \equiv \frac{1}{\Delta p_\mathrm{T}\Delta y}\sigma_\mathrm{bin}^{\Upsilon\to\mu^+\mu^-} = \frac{1}{\Delta p_\mathrm{T}\Delta y}\frac{N_{\Upsilon\to\mu^+\mu^-}}{\mathcal{L}}, \tag{1}$$

where $\mathcal{B}_\Upsilon$ is the branching fraction of the $\Upsilon\to\mu^+\mu^-$ decay, Δy and Δp_T are the rapidity and p_T bin sizes, $\sigma_\mathrm{bin}^{\Upsilon\to\mu^+\mu^-}$ is a production cross-section for $\Upsilon\to\mu^+\mu^-$ events in the given (p_T, y) bin, $N_{\Upsilon\to\mu^+\mu^-}$ is the efficiency-corrected number of $\Upsilon\to\mu^+\mu^-$ decays and $\mathcal{L}$ is the integrated luminosity. Given the sizeable uncertainty on the dimuon branching fractions of the Υ mesons [42], the measurement of the production cross-section multiplied by the dimuon branching fraction is presented, as in previous LHCb measurements [21–23].

A large part of the theoretical and experimental uncertainties cancel in the ratios of production cross-sections of various Υ mesons, defined for a given (p_T, y) bin as

$$\mathscr{R}_{\mathrm{i,j}} \equiv \frac{\sigma_\mathrm{bin}^{\Upsilon(\mathrm{iS})\to\mu^+\mu^-}}{\sigma_\mathrm{bin}^{\Upsilon(\mathrm{jS})\to\mu^+\mu^-}} = \frac{N_{\Upsilon(\mathrm{iS})\to\mu^+\mu^-}}{N_{\Upsilon(\mathrm{jS})\to\mu^+\mu^-}}. \tag{2}$$

The evolution of the production cross-sections as a function of pp collision energy is studied using the ratio

$$\mathscr{R}_{8/7} \equiv \frac{\sigma_\mathrm{bin}^{\Upsilon\to\mu^+\mu^-}\Big|_{\sqrt{s}=8\,\mathrm{TeV}}}{\sigma_\mathrm{bin}^{\Upsilon\to\mu^+\mu^-}\Big|_{\sqrt{s}=7\,\mathrm{TeV}}}. \tag{3}$$

The signal yields $N_{\Upsilon\to\mu^+\mu^-}$ in each (p_T, y) bin are determined from an unbinned extended maximum likelihood fit to the dimuon mass spectrum of the selected candidates within the range $8.5 < m_{\mu^+\mu^-} < 12.5$ GeV/c^2. The correction for efficiency is embedded in the fit procedure. Each dimuon candidate is given a weight calculated as $1/\varepsilon^\mathrm{tot}$, where ε^tot is the total efficiency, which is determined for each $\Upsilon\to\mu^+\mu^-$ candidate as

$$\varepsilon^\mathrm{tot} = \varepsilon^\mathrm{rec\&sel} \times \varepsilon^\mathrm{trg} \times \varepsilon^\mathrm{\mu ID}, \tag{4}$$

where $\varepsilon^\mathrm{rec\&sel}$ is the reconstruction and selection efficiency, ε^trg is the trigger efficiency and $\varepsilon^\mathrm{\mu ID}$ is the efficiency of the muon identification criteria. The efficiencies $\varepsilon^\mathrm{rec\&sel}$ and ε^trg are determined using simulation, and corrected using data-driven techniques to account for small differences in the muon reconstruction efficiency between data and simulation [39, 40]. The efficiency of the muon identification criteria $\varepsilon^\mathrm{\mu ID}$ is measured directly from data using a large sample of low-background $\mathrm{J/\psi}\to\mu^+\mu^-$ events. All efficiencies are evaluated as functions of the muon and dimuon kinematics. The mean total efficiency $\langle\varepsilon^\mathrm{tot}\rangle$ reaches a maximum of about 45% for the region $15 < p_\mathrm{T} < 20\,\mathrm{GeV}/c$, $3.0 < y < 3.5$, and drops down to 10% at high p_T and large y, with the average efficiency being about 30%.

In each (p_T, y) bin, the dimuon mass distribution is described by the sum of three Crystal Ball functions [43], one for each of the Υ(1S), Υ(2S) and Υ(3S) signals, and the product of an exponential function with a second-order polynomial for the combinatorial background. The mean value and the resolution of the Crystal Ball function describing

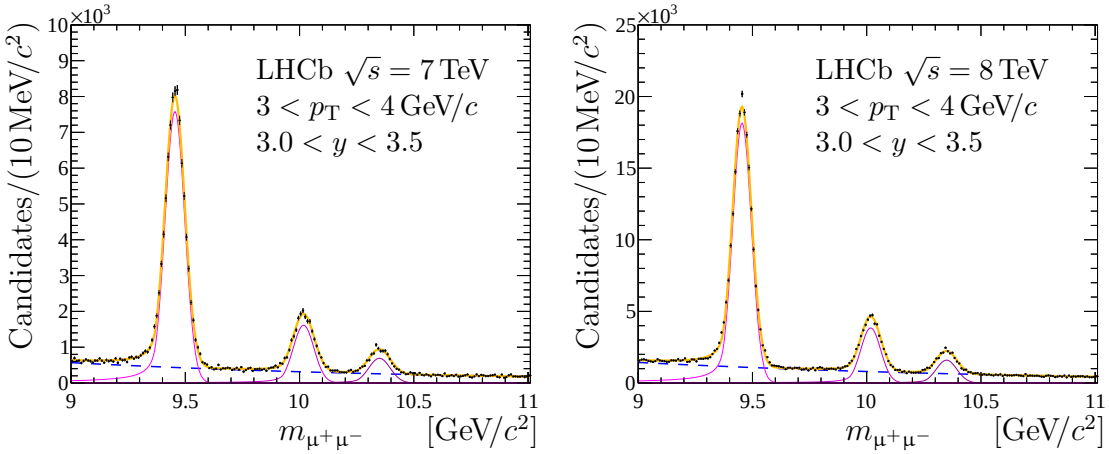

Figure 1: Efficiency-corrected dimuon mass distributions for (left) $\sqrt{s} = 7\,\text{TeV}$ and (right) $\sqrt{s} = 8\,\text{TeV}$ samples in the region $3 < p_\text{T} < 4\,\text{GeV}/c$, $3.0 < y < 3.5$. The thick dark yellow solid curves show the result of the fits, as described in the text. The three peaks, shown with thin magenta solid lines, correspond to the $\Upsilon(1S)$, $\Upsilon(2S)$ and $\Upsilon(3S)$ signals (left to right). The background component is indicated with a blue dashed line. To show the signal peaks clearly, the range of the dimuon mass shown is narrower than that used in the fit.

the mass distribution of the $\Upsilon(1S)$ meson are free fit parameters. For the $\Upsilon(2S)$ and $\Upsilon(3S)$ mesons the mass differences $m(\Upsilon(2S)) - m(\Upsilon(1S))$ and $m(\Upsilon(3S)) - m(\Upsilon(1S))$ are fixed to the known values [42], while the resolutions are fixed to the value of the resolution of the $\Upsilon(1S)$ signal, scaled by the ratio of the masses of the $\Upsilon(2S)$ and $\Upsilon(3S)$ to the $\Upsilon(1S)$ meson. The tail parameters of the Crystal Ball function describing the radiative tail are fixed from studies of simulated samples.

The fits are performed independently on the efficiency-corrected dimuon mass distributions in each (p_T,y) bin. As an example, Fig. 1 shows the results of the fits in the region $3 < p_\text{T} < 4\,\text{GeV}/c$ and $3.0 < y < 3.5$. For each bin the position and the resolution of the $\Upsilon(1S)$ signal is found to be consistent between $\sqrt{s} = 7$ and $8\,\text{TeV}$ data sets. The resolution varies between $33\,\text{MeV}/c^2$ in the region of low p_T and small rapidity and $90\,\text{MeV}/c^2$ for the high p_T and large y region, with the average value being close to $42\,\text{MeV}/c^2$. The total signal yields are obtained by summing the signal yields over all (p_T, y) bins and are summarised in Table 1.

4 Systematic uncertainties

The systematic uncertainties are summarised in Table 2, separately for the measurement of the cross-sections and of their ratios.

The uncertainty related to the mass model describing the shape of the dimuon mass distribution is studied by varying the fit range and the signal and background parametrisation used in the fit model. The fit range is varied by moving the upper edge

Table 1: Efficiency-corrected signal yields for data samples accumulated at $\sqrt{s} = 7$ and 8 TeV summed over the full kinematic range $p_{\mathrm{T}} < 30\,\mathrm{GeV}/c$, $2.0 < y < 4.5$. The uncertainties are statistical only.

	$\sqrt{s} = 7\,\mathrm{TeV}$	$\sqrt{s} = 8\,\mathrm{TeV}$
$N_{\Upsilon(1\mathrm{S})\to\mu^+\mu^-}$	$(2639.8 \pm 3.7) \cdot 10^3$	$(6563.1 \pm 6.3) \cdot 10^3$
$N_{\Upsilon(2\mathrm{S})\to\mu^+\mu^-}$	$(667.3 \pm 2.2) \cdot 10^3$	$(1674.3 \pm 3.5) \cdot 10^3$
$N_{\Upsilon(3\mathrm{S})\to\mu^+\mu^-}$	$(328.8 \pm 1.5) \cdot 10^3$	$(786.6 \pm 2.6) \cdot 10^3$

Table 2: Summary of relative systematic uncertainties (in %) for the differential production cross-sections, their ratios, integrated cross-sections and the ratios $\mathscr{R}_{8/7}$. The ranges indicate variations depending on the (p_{T}, y) bin and the Υ state.

Source	$\sigma_{\mathrm{bin}}^{\Upsilon\to\mu^+\mu^-}$	$\mathscr{R}_{\mathrm{i,j}}$	$\sigma^{\Upsilon\to\mu^+\mu^-}$	$\mathscr{R}_{8/7}$
Fit model and range	$0.1 - 4.8$	$0.1 - 2.9$	0.1	—
Efficiency correction	$0.2 - 0.6$	$0.1 - 1.1$	0.4	—
Efficiency uncertainty	$0.2 - 0.3$	—	0.2	0.3
Muon identification	$0.3 - 0.5$	—	0.3	0.2
Data-simulation agreement				
Radiative tails	1.0	—	1.0	—
Selection efficiency	1.0	0.5	1.0	0.5
Tracking efficiency	$0.5 \oplus (2 \times 0.4)$	—	$0.5 \oplus (2 \times 0.4)$	—
Trigger efficiency	2.0	—	2.0	1.0
Luminosity	$1.7\,(\sqrt{s} = 7\,\mathrm{TeV})$ $1.2\,(\sqrt{s} = 8\,\mathrm{TeV})$	—	$1.7\,(\sqrt{s} = 7\,\mathrm{TeV})$ $1.2\,(\sqrt{s} = 8\,\mathrm{TeV})$	1.4

from 12.5 to $11.5\,\mathrm{GeV}/c^2$; the degree of the polynomial function used in the estimation of the background is varied between zeroth and the third order. Also the tail parameters of the Crystal Ball function are allowed to vary in the fit. In addition, the constraints on the difference in the Υ signal peak positions are removed for all bins with high signal yields. The maximum relative difference in the number of signal events is taken as a systematic uncertainty arising from the choice of the fit model.

As an alternative to the determination of the signal yields from efficiency-corrected data, the method employed in Ref. [21] is used. In this method the efficiency-corrected yields for each (p_{T}, y) bin are calculated using the *sPlot* technique [44]. The difference between this method and the nominal one is taken as a systematic uncertainty on the efficiency correction.

Reconstruction, selection and trigger efficiencies in Eq. (4) are obtained using simulated samples. The uncertainties due to the finite size of these samples are propagated to the measurement using a large number of pseudoexperiments. The same technique is used

for the propagation of the uncertainties on the muon identification efficiency determined from large low-background samples of $J/\psi \to \mu^+\mu^-$ decays.

Several systematic uncertainties are assigned to account for possible imperfections in the simulated samples. The possible mismodelling of the bremsstrahlung simulation for the radiative tail and its effect on the signal shape has been estimated in previous LHCb analyses [23] and leads to an additional uncertainty of 1.0% on the cross-section.

Good agreement between data and simulation is observed for all variables used in the selection. The small differences seen would affect the efficiencies by less than 1.0%, which is conservatively taken as the systematic uncertainty to account for the disagreement between data and simulation.

The efficiency is corrected using data-driven techniques to account for small differences in the tracking efficiency between data and simulation [39, 40]. The uncertainty in the correction factor is propagated to the cross-section measurement using pseudoexperiments and results in a global 0.5% systematic uncertainty plus an additional uncertainty of 0.4% per track.

The systematic uncertainty associated with the trigger requirements is assessed by studying the performance of the dimuon trigger for $\Upsilon(1S)$ events selected using the single muon high-p_T trigger [32] in data and simulation. The comparison is perfomed in bins of the $\Upsilon(1S)$ meson transverse momentum and rapidity and the largest observed difference of 2.0% is assigned as the systematic uncertainty associated with the imperfection of trigger simulation.

The luminosity measurement was calibrated during dedicated data taking periods, using both van der Meer scans [45] and a beam-gas imaging method [46, 47]. The absolute luminosity scale is determined with 1.7 (1.2)% uncertainty for the sample collected at $\sqrt{s} = 7\,(8)$ TeV, of which the beam-gas resolution, the spread of the measurements and the detector alignment are the largest contributions [47–49]. The ratio of absolute luminosities for samples accumulated at $\sqrt{s} = 7$ and 8 TeV is known with a 1.4% uncertainty.

The total systematic uncertainty in each (p_T, y) bin is the sum in quadrature of the individual components described above. For the integrated production cross-section the systematic uncertainty is estimated by taking into account bin-to-bin correlations. Several systematic uncertainties cancel or significantly reduce in the measurement of the ratios $\mathscr{R}_{i,j}$ and $\mathscr{R}_{8/7}$, as shown in Table 2.

The production cross-sections are measured at centre-of-mass energies of 7 and 8 TeV, where the actual beam energy for pp collisions is known with a precision of 0.65% [50]. Assuming a linear dependence of the production cross-section on the pp collision energy, and using the measured production cross-sections at $\sqrt{s} = 7\,(8)$ TeV, the change in the production cross-section due to the imprecise knowledge of the beam energy is estimated to be 1.4 (1.2)%. The effect is strongly correlated between $\sqrt{s} = 7$ and 8 TeV data and will therefore mostly cancel in the measurement of the ratio of cross-sections at the two energies.

The efficiency is dependent on the polarisation of the Υ mesons. The polarisation of the Υ mesons produced in pp collisions at $\sqrt{s} = 7$ TeV at high p_T and central rapidity has been studied by the CMS collaboration [51] in the centre-of-mass helicity, Collins-Soper [52]

and the perpendicular helicity frames. No evidence of significant transverse or longitudinal polarisation has been observed for the region $10 < p_{\rm T} < 50\,{\rm GeV}/c$, $|y| < 1.2$. Therefore, results are quoted under the assumption of unpolarised production of Υ mesons and no corresponding systematic uncertainty is assigned on the cross-section. Under the assumption of transversely polarised Υ mesons with $\lambda_\vartheta = 0.2$ in the LHCb kinematic region,[1] the total production cross-section would result in an increase of 3%, with the largest local increase of around 6% occuring in the low $p_{\rm T}$ region ($p_{\rm T} < 3\,{\rm GeV}/c$), both for small ($y < 2.5$) and large ($y > 4.0$) rapidities.

5 Results

The double-differential production cross-sections multiplied by the dimuon branching fractions for the Υ mesons are shown in Fig. 2. The corresponding production cross-section $\sigma_{\rm bin}^{\Upsilon\to\mu^+\mu^-}$ in $(p_{\rm T}, y)$ bins are presented in Tables 3, 4 and 5 for $\sqrt{s} = 7\,{\rm TeV}$ and Tables 6, 7 and 8 for $\sqrt{s} = 8\,{\rm TeV}$. The cross-sections integrated over y as a function of $p_{\rm T}$ and integrated over $p_{\rm T}$ as a function of rapidity are shown in Figs. 3 and 4, respectively.

The transverse momentum spectra are fit using a Tsallis function [53]

$$\frac{{\rm d}\sigma}{p_{\rm T}\,{\rm d}p_{\rm T}} \propto \left(1 + \frac{E_{\rm T}^{\rm kin}}{n\,T}\right)^{-n}, \tag{5}$$

where $E_{\rm T}^{\rm kin} \equiv \sqrt{m_\Upsilon^2 + p_{\rm T}^2} - m_\Upsilon$ is the transverse kinetic energy, the power n and the temperature parameter T are free parameters, and m_Υ is the known mass of a Υ meson [42]. This function has a power-law asymptotic behaviour $\propto p_{\rm T}^{-n}$ for high $p_{\rm T}$ as expected for hard scattering processes. It has been successfully applied to fit $p_{\rm T}$ spectra [54–57] in wide ranges of particle species, processes and kinematics. A fit with the Tsallis distribution for the range $6 < p_{\rm T} < 30\,{\rm GeV}/c$ is superimposed on the differential cross-sections in Fig. 3. The fit quality is good for all cases. The fitted values of the parameters n and T are listed in Table 9. The parameter n for all cases is close to 8, compatible with the high $p_{\rm T}$ asymptotic behaviour expected by the CS model [3,4,58–60]. The temperature parameters T show little dependence on $\sqrt{s}$ and increase with the mass of Υ state.

The shapes of the rapidity spectra are compared with the CO model prediction in the region $2.5 < y < 4.0$ and are fitted using the function given by Eq. (1) of Ref. [63], with free normalisation constants. The fit result, as well as the extrapolation to the full kinematic range $2.0 < y < 4.5$, is presented in Fig. 4. The quality of the fit is good for all cases.

The integrated production cross-sections multiplied by the dimuon branching fractions in the full range $p_{\rm T} < 30\,{\rm GeV}/c$ and $2.0 < y < 4.5$ at $\sqrt{s} = 7$ and $8\,{\rm TeV}$ are reported in Table 10, where the first uncertainties are statistical and the second systematic. The same measurements are also shown integrated over the reduced range $p_{\rm T} < 15\,{\rm GeV}/c$ in the same rapidity range, to allow the comparison with previous measurements [22, 23].

[1] The CMS measurements for $\Upsilon(1{\rm S})$ mesons are consistent with small transverse polarisation in the helicity frame with the central values for the polarisation parameter $0 \lesssim \lambda_\vartheta \lesssim 0.2$ [51].

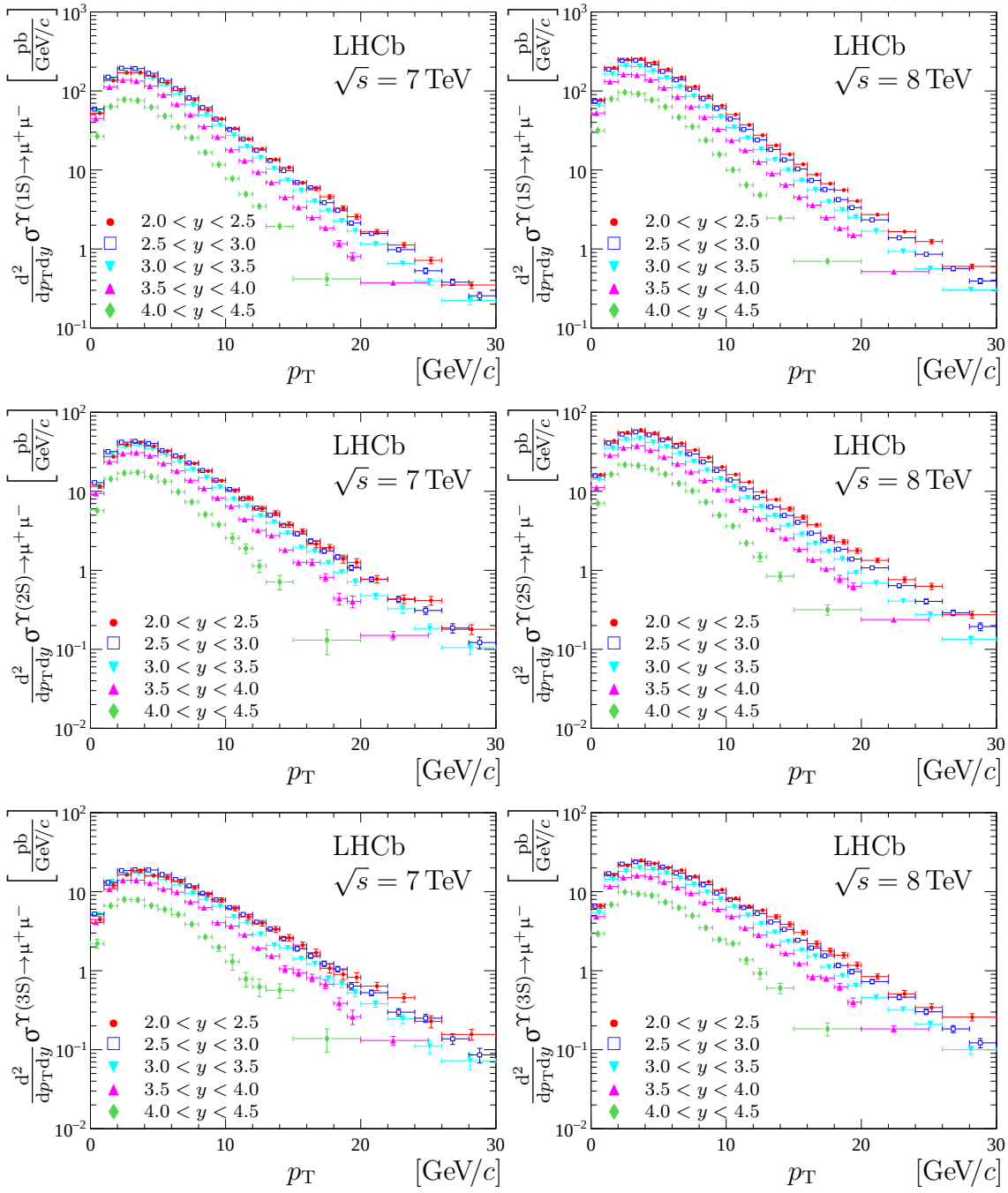

Figure 2: Double differential cross-sections $\dfrac{\mathrm{d}^2}{\mathrm{d}p_\mathrm{T}\,\mathrm{d}y}\sigma^{\Upsilon\to\mu^+\mu^-}$ for (top) $\Upsilon(1S)$, (middle) $\Upsilon(2S)$ and (bottom) $\Upsilon(3S)$ at (left) $\sqrt{s} = 7\,\text{TeV}$ and (right) $\sqrt{s} = 8\,\text{TeV}$. The error bars indicate the sum in quadrature of the statistical and systematic uncertainties. The rapidity ranges $2.0 < y < 2.5$, $2.5 < y < 3.0$, $3.0 < y < 3.5$, $3.5 < y < 4.0$ and $4.0 < y < 4.5$ are shown with red filled circles, blue open squares, cyan downward triangles, magenta upward triangles and green diamonds, respectively. Some data points are displaced from the bin centres to improve visibility.

Table 3: Production cross-section $\sigma_{\rm bin}^{\Upsilon(1S)\to\mu^+\mu^-}$ [pb] in $(p_{\rm T}, y)$ bins for $\sqrt{s} = 7\,\text{TeV}$. The first uncertainties are statistical and the second are the uncorrelated component of the systematic uncertainties. The overall correlated systematic uncertainty is 3.1% and is not included in the numbers in the table. The horizontal lines indicate bin boundaries.

$p_{\rm T}$ [GeV/c]	$2.0 < y < 2.5$	$2.5 < y < 3.0$	$3.0 < y < 3.5$	$3.5 < y < 4.0$	$4.0 < y < 4.5$
$0-1$	$26.1 \pm 0.5 \pm 0.3$	$29.55 \pm 0.30 \pm 0.11$	$27.0 \pm 0.3 \pm 0.4$	$22.5 \pm 0.3 \pm 0.7$	$13.4 \pm 0.4 \pm 0.2$
$1-2$	$67.9 \pm 0.8 \pm 1.0$	$74.9 \pm 0.5 \pm 0.4$	$68.8 \pm 0.4 \pm 0.5$	$56.0 \pm 0.4 \pm 0.3$	$31.8 \pm 0.6 \pm 0.1$
$2-3$	$85.0 \pm 0.8 \pm 0.7$	$97.0 \pm 0.6 \pm 0.4$	$85.2 \pm 0.5 \pm 0.3$	$68.5 \pm 0.5 \pm 0.8$	$38.9 \pm 0.6 \pm 1.0$
$3-4$	$85.3 \pm 0.8 \pm 1.7$	$96.0 \pm 0.6 \pm 0.4$	$84.2 \pm 0.5 \pm 0.1$	$66.7 \pm 0.5 \pm 0.4$	$37.7 \pm 0.6 \pm 0.3$
$4-5$	$77.2 \pm 0.8 \pm 0.3$	$83.7 \pm 0.5 \pm 0.2$	$72.2 \pm 0.4 \pm 0.3$	$57.6 \pm 0.4 \pm 0.8$	$31.0 \pm 0.5 \pm 0.2$
$5-6$	$63.4 \pm 0.7 \pm 1.1$	$68.1 \pm 0.5 \pm 0.3$	$59.4 \pm 0.4 \pm 0.4$	$44.6 \pm 0.4 \pm 0.3$	$24.0 \pm 0.5 \pm 0.1$
$6-7$	$50.9 \pm 0.6 \pm 0.8$	$53.6 \pm 0.4 \pm 0.4$	$45.5 \pm 0.4 \pm 0.4$	$34.0 \pm 0.3 \pm 0.2$	$17.6 \pm 0.4 \pm 0.4$
$7-8$	$38.7 \pm 0.5 \pm 0.6$	$40.9 \pm 0.4 \pm 0.4$	$33.4 \pm 0.3 \pm 0.2$	$25.0 \pm 0.3 \pm 0.2$	$12.78 \pm 0.33 \pm 0.04$
$8-9$	$28.6 \pm 0.5 \pm 0.4$	$30.8 \pm 0.3 \pm 0.3$	$24.76 \pm 0.25 \pm 0.25$	$17.74 \pm 0.24 \pm 0.12$	$8.31 \pm 0.27 \pm 0.14$
$9-10$	$22.2 \pm 0.4 \pm 0.3$	$22.05 \pm 0.26 \pm 0.13$	$18.39 \pm 0.22 \pm 0.14$	$13.10 \pm 0.21 \pm 0.12$	$5.83 \pm 0.23 \pm 0.06$
$10-11$	$16.7 \pm 0.4 \pm 0.2$	$16.35 \pm 0.22 \pm 0.06$	$13.71 \pm 0.18 \pm 0.03$	$8.99 \pm 0.17 \pm 0.04$	$3.9 \pm 0.2 \pm 0.3$
$11-12$	$12.3 \pm 0.3 \pm 0.2$	$12.32 \pm 0.19 \pm 0.16$	$9.81 \pm 0.16 \pm 0.02$	$6.55 \pm 0.14 \pm 0.08$	$2.48 \pm 0.17 \pm 0.02$
$12-13$	$9.24 \pm 0.26 \pm 0.15$	$8.92 \pm 0.16 \pm 0.05$	$7.08 \pm 0.13 \pm 0.01$	$4.68 \pm 0.12 \pm 0.03$	$1.73 \pm 0.16 \pm 0.04$
$13-14$	$6.78 \pm 0.22 \pm 0.09$	$6.60 \pm 0.13 \pm 0.08$	$5.14 \pm 0.11 \pm 0.03$	$3.47 \pm 0.10 \pm 0.02$	$1.93 \pm 0.19 \pm 0.07$
$14-15$	$5.38 \pm 0.19 \pm 0.10$	$4.91 \pm 0.11 \pm 0.04$	$3.70 \pm 0.09 \pm 0.07$	$2.25 \pm 0.08 \pm 0.04$	
$15-16$	$3.44 \pm 0.15 \pm 0.02$	$3.46 \pm 0.10 \pm 0.04$	$2.74 \pm 0.08 \pm 0.01$	$1.68 \pm 0.07 \pm 0.02$	
$16-17$	$2.91 \pm 0.14 \pm 0.07$	$2.97 \pm 0.09 \pm 0.03$	$1.99 \pm 0.07 \pm 0.01$	$1.25 \pm 0.06 \pm 0.03$	
$17-18$	$2.29 \pm 0.12 \pm 0.02$	$1.93 \pm 0.07 \pm 0.01$	$1.52 \pm 0.06 \pm 0.01$	$0.92 \pm 0.06 \pm 0.01$	$1.04 \pm 0.17 \pm 0.03$
$18-19$	$1.64 \pm 0.10 \pm 0.04$	$1.54 \pm 0.06 \pm 0.01$	$1.13 \pm 0.05 \pm 0.01$	$0.58 \pm 0.05 \pm 0.03$	
$19-20$	$1.28 \pm 0.08 \pm 0.02$	$1.06 \pm 0.05 \pm 0.01$	$0.84 \pm 0.05 \pm 0.01$	$0.40 \pm 0.04 \pm 0.02$	
$20-21$	$1.65 \pm 0.10 \pm 0.05$	$1.57 \pm 0.06 \pm 0.01$	$1.15 \pm 0.05 \pm 0.01$	$0.94 \pm 0.06 \pm 0.01$	
$21-22$					
$22-23$	$1.12 \pm 0.08 \pm 0.01$	$0.98 \pm 0.05 \pm 0.01$	$0.65 \pm 0.04 \pm 0.02$		
$23-24$					
$24-25$	$0.72 \pm 0.06 \pm 0.01$	$0.53 \pm 0.04 \pm 0.01$	$0.39 \pm 0.03 \pm 0.01$		
$25-26$					
$26-27$	$0.70 \pm 0.06 \pm 0.01$	$0.38 \pm 0.03 \pm 0.01$	$0.45 \pm 0.04 \pm 0.03$		
$27-28$					
$28-29$		$0.26 \pm 0.03 \pm 0.01$			
$29-30$					

Table 4: Production cross-section $\sigma_{\rm bin}^{\Upsilon(2S)\to\mu^+\mu^-}$ [pb] in $(p_{\rm T}, y)$ bins for $\sqrt{s} = 7\,\text{TeV}$. The first uncertainties are statistical and the second are the uncorrelated component of the systematic uncertainties. The overall correlated systematic uncertainty is 3.1% and is not included in the numbers in the table. The horizontal lines indicate bin boundaries.

$p_{\rm T}$ [GeV/c]	$2.0 < y < 2.5$	$2.5 < y < 3.0$	$3.0 < y < 3.5$	$3.5 < y < 4.0$	$4.0 < y < 4.5$
$0 - 1$	$5.80 \pm 0.25 \pm 0.12$	$6.44 \pm 0.16 \pm 0.04$	$5.69 \pm 0.14 \pm 0.12$	$4.71 \pm 0.14 \pm 0.24$	$2.86 \pm 0.19 \pm 0.10$
$1 - 2$	$13.7 \pm 0.4 \pm 0.4$	$15.95 \pm 0.25 \pm 0.13$	$14.40 \pm 0.23 \pm 0.14$	$11.87 \pm 0.22 \pm 0.10$	$7.16 \pm 0.30 \pm 0.03$
$2 - 3$	$19.5 \pm 0.4 \pm 0.3$	$20.98 \pm 0.29 \pm 0.13$	$18.35 \pm 0.25 \pm 0.10$	$15.1 \pm 0.2 \pm 0.3$	$8.5 \pm 0.3 \pm 0.4$
$3 - 4$	$20.7 \pm 0.5 \pm 0.7$	$21.49 \pm 0.29 \pm 0.13$	$19.22 \pm 0.26 \pm 0.06$	$15.42 \pm 0.25 \pm 0.13$	$8.72 \pm 0.31 \pm 0.12$
$4 - 5$	$18.6 \pm 0.4 \pm 0.1$	$20.16 \pm 0.28 \pm 0.07$	$17.40 \pm 0.24 \pm 0.14$	$14.1 \pm 0.2 \pm 0.4$	$7.67 \pm 0.28 \pm 0.13$
$5 - 6$	$16.2 \pm 0.4 \pm 0.4$	$16.37 \pm 0.26 \pm 0.11$	$14.47 \pm 0.22 \pm 0.18$	$11.26 \pm 0.21 \pm 0.11$	$6.67 \pm 0.26 \pm 0.04$
$6 - 7$	$13.5 \pm 0.4 \pm 0.4$	$14.04 \pm 0.24 \pm 0.13$	$11.84 \pm 0.20 \pm 0.17$	$9.07 \pm 0.19 \pm 0.10$	$4.91 \pm 0.22 \pm 0.19$
$7 - 8$	$11.3 \pm 0.3 \pm 0.3$	$11.42 \pm 0.21 \pm 0.20$	$9.37 \pm 0.17 \pm 0.11$	$6.92 \pm 0.17 \pm 0.13$	$3.67 \pm 0.19 \pm 0.04$
$8 - 9$	$9.04 \pm 0.29 \pm 0.17$	$9.17 \pm 0.19 \pm 0.12$	$7.43 \pm 0.15 \pm 0.12$	$5.46 \pm 0.15 \pm 0.07$	$2.55 \pm 0.16 \pm 0.08$
$9 - 10$	$6.82 \pm 0.25 \pm 0.15$	$6.91 \pm 0.16 \pm 0.05$	$5.64 \pm 0.13 \pm 0.09$	$4.12 \pm 0.13 \pm 0.09$	$1.88 \pm 0.15 \pm 0.03$
$10 - 11$	$5.17 \pm 0.22 \pm 0.11$	$5.28 \pm 0.13 \pm 0.04$	$3.96 \pm 0.11 \pm 0.01$	$3.23 \pm 0.11 \pm 0.02$	$1.28 \pm 0.13 \pm 0.13$
$11 - 12$	$4.10 \pm 0.19 \pm 0.11$	$4.03 \pm 0.12 \pm 0.08$	$3.23 \pm 0.10 \pm 0.02$	$2.20 \pm 0.09 \pm 0.04$	$0.95 \pm 0.13 \pm 0.01$
$12 - 13$	$3.02 \pm 0.16 \pm 0.09$	$3.07 \pm 0.10 \pm 0.04$	$2.43 \pm 0.08 \pm 0.01$	$1.60 \pm 0.08 \pm 0.01$	$0.57 \pm 0.10 \pm 0.02$
$13 - 14$	$2.66 \pm 0.15 \pm 0.07$	$2.50 \pm 0.09 \pm 0.04$	$2.02 \pm 0.07 \pm 0.02$	$1.38 \pm 0.07 \pm 0.02$	$0.71 \pm 0.14 \pm 0.03$
$14 - 15$	$1.90 \pm 0.12 \pm 0.07$	$1.85 \pm 0.07 \pm 0.03$	$1.47 \pm 0.06 \pm 0.04$	$0.90 \pm 0.06 \pm 0.03$	
$15 - 16$	$1.56 \pm 0.11 \pm 0.01$	$1.45 \pm 0.07 \pm 0.02$	$0.97 \pm 0.05 \pm 0.01$	$0.63 \pm 0.05 \pm 0.01$	
$16 - 17$	$1.08 \pm 0.09 \pm 0.05$	$1.17 \pm 0.06 \pm 0.02$	$0.87 \pm 0.05 \pm 0.01$	$0.63 \pm 0.05 \pm 0.03$	
$17 - 18$	$0.97 \pm 0.08 \pm 0.01$	$0.88 \pm 0.05 \pm 0.01$	$0.62 \pm 0.04 \pm 0.01$	$0.41 \pm 0.04 \pm 0.01$	$0.33 \pm 0.11 \pm 0.01$
$18 - 19$	$0.70 \pm 0.07 \pm 0.03$	$0.74 \pm 0.05 \pm 0.01$	$0.48 \pm 0.04 \pm 0.01$	$0.22 \pm 0.03 \pm 0.02$	
$19 - 20$	$0.63 \pm 0.07 \pm 0.02$	$0.54 \pm 0.04 \pm 0.01$	$0.36 \pm 0.03 \pm 0.01$	$0.20 \pm 0.03 \pm 0.01$	
$20 - 21$	$0.77 \pm 0.07 \pm 0.04$	$0.77 \pm 0.05 \pm 0.01$	$0.48 \pm 0.04 \pm 0.01$		
$21 - 22$					
$22 - 23$	$0.43 \pm 0.05 \pm 0.01$	$0.43 \pm 0.04 \pm 0.01$	$0.33 \pm 0.03 \pm 0.01$	$0.38 \pm 0.04 \pm 0.01$	
$23 - 24$					
$24 - 25$	$0.41 \pm 0.05 \pm 0.01$	$0.31 \pm 0.03 \pm 0.01$	$0.18 \pm 0.02 \pm 0.01$		
$25 - 26$					
$26 - 27$	$0.36 \pm 0.05 \pm 0.01$	$0.19 \pm 0.02 \pm 0.01$	$0.21 \pm 0.03 \pm 0.02$		
$27 - 28$					
$28 - 29$		$0.12 \pm 0.02 \pm 0.01$			
$29 - 30$					

Table 5: Production cross-section $\sigma_{\rm bin}^{\Upsilon(3S)\to\mu^+\mu^-}$ [pb] in $(p_{\rm T}, y)$ bins for $\sqrt{s} = 7\,\text{TeV}$. The first uncertainties are statistical and the second are the uncorrelated component of the systematic uncertainties. The overall correlated systematic uncertainty is 3.1% and is not included in the numbers in the table. The horizontal lines indicate bin boundaries.

$p_{\rm T}$ [GeV/c]	$2.0 < y < 2.5$	$2.5 < y < 3.0$	$3.0 < y < 3.5$	$3.5 < y < 4.0$	$4.0 < y < 4.5$
$0 - 1$	$2.22 \pm 0.17 \pm 0.05$	$2.61 \pm 0.11 \pm 0.02$	$2.54 \pm 0.11 \pm 0.08$	$2.05 \pm 0.10 \pm 0.12$	$1.10 \pm 0.13 \pm 0.05$
$1 - 2$	$5.99 \pm 0.28 \pm 0.17$	$6.58 \pm 0.18 \pm 0.08$	$6.61 \pm 0.17 \pm 0.09$	$5.40 \pm 0.16 \pm 0.07$	$3.33 \pm 0.22 \pm 0.01$
$2 - 3$	$8.22 \pm 0.31 \pm 0.11$	$9.25 \pm 0.21 \pm 0.08$	$8.17 \pm 0.19 \pm 0.03$	$6.98 \pm 0.18 \pm 0.17$	$3.99 \pm 0.23 \pm 0.24$
$3 - 4$	$9.3 \pm 0.3 \pm 0.3$	$9.46 \pm 0.22 \pm 0.06$	$8.53 \pm 0.19 \pm 0.01$	$6.99 \pm 0.18 \pm 0.05$	$3.94 \pm 0.22 \pm 0.06$
$4 - 5$	$8.00 \pm 0.31 \pm 0.02$	$9.42 \pm 0.21 \pm 0.05$	$7.84 \pm 0.18 \pm 0.03$	$6.40 \pm 0.17 \pm 0.21$	$3.33 \pm 0.20 \pm 0.05$
$5 - 6$	$7.7 \pm 0.3 \pm 0.2$	$8.25 \pm 0.20 \pm 0.05$	$7.10 \pm 0.17 \pm 0.10$	$5.42 \pm 0.16 \pm 0.08$	$2.98 \pm 0.18 \pm 0.02$
$6 - 7$	$6.84 \pm 0.27 \pm 0.20$	$7.13 \pm 0.18 \pm 0.09$	$6.17 \pm 0.15 \pm 0.10$	$4.93 \pm 0.15 \pm 0.07$	$2.57 \pm 0.17 \pm 0.14$
$7 - 8$	$5.68 \pm 0.25 \pm 0.15$	$5.93 \pm 0.16 \pm 0.11$	$4.75 \pm 0.13 \pm 0.07$	$3.72 \pm 0.13 \pm 0.08$	$1.94 \pm 0.15 \pm 0.03$
$8 - 9$	$4.63 \pm 0.22 \pm 0.11$	$4.77 \pm 0.14 \pm 0.07$	$3.99 \pm 0.12 \pm 0.08$	$3.15 \pm 0.12 \pm 0.04$	$1.33 \pm 0.13 \pm 0.04$
$9 - 10$	$3.93 \pm 0.20 \pm 0.11$	$3.96 \pm 0.13 \pm 0.04$	$3.28 \pm 0.10 \pm 0.05$	$2.03 \pm 0.09 \pm 0.05$	$0.99 \pm 0.11 \pm 0.01$
$10 - 11$	$3.08 \pm 0.18 \pm 0.06$	$3.15 \pm 0.11 \pm 0.03$	$2.38 \pm 0.09 \pm 0.01$	$1.84 \pm 0.09 \pm 0.01$	$0.65 \pm 0.10 \pm 0.10$
$11 - 12$	$2.40 \pm 0.15 \pm 0.07$	$2.58 \pm 0.10 \pm 0.06$	$2.02 \pm 0.08 \pm 0.01$	$1.43 \pm 0.08 \pm 0.03$	$0.39 \pm 0.08 \pm 0.01$
$12 - 13$	$2.00 \pm 0.14 \pm 0.06$	$2.06 \pm 0.08 \pm 0.02$	$1.43 \pm 0.07 \pm 0.01$	$0.97 \pm 0.06 \pm 0.01$	$0.31 \pm 0.08 \pm 0.01$
$13 - 14$	$1.67 \pm 0.12 \pm 0.06$	$1.69 \pm 0.07 \pm 0.03$	$1.05 \pm 0.06 \pm 0.01$	$0.77 \pm 0.05 \pm 0.01$	$0.56 \pm 0.11 \pm 0.02$
$14 - 15$	$1.31 \pm 0.11 \pm 0.04$	$1.28 \pm 0.06 \pm 0.02$	$0.97 \pm 0.05 \pm 0.02$	$0.53 \pm 0.05 \pm 0.01$	
$15 - 16$	$1.05 \pm 0.09 \pm 0.01$	$0.95 \pm 0.06 \pm 0.01$	$0.71 \pm 0.04 \pm 0.01$	$0.47 \pm 0.04 \pm 0.01$	
$16 - 17$	$0.84 \pm 0.08 \pm 0.03$	$0.77 \pm 0.05 \pm 0.01$	$0.61 \pm 0.04 \pm 0.01$	$0.41 \pm 0.04 \pm 0.01$	
$17 - 18$	$0.54 \pm 0.07 \pm 0.01$	$0.61 \pm 0.04 \pm 0.01$	$0.40 \pm 0.03 \pm 0.01$	$0.34 \pm 0.04 \pm 0.01$	$0.35 \pm 0.11 \pm 0.01$
$18 - 19$	$0.45 \pm 0.06 \pm 0.02$	$0.53 \pm 0.04 \pm 0.01$	$0.34 \pm 0.03 \pm 0.01$	$0.19 \pm 0.03 \pm 0.01$	
$19 - 20$	$0.41 \pm 0.05 \pm 0.01$	$0.32 \pm 0.03 \pm 0.01$	$0.26 \pm 0.03 \pm 0.01$	$0.13 \pm 0.03 \pm 0.01$	
$20 - 21$	$0.64 \pm 0.07 \pm 0.02$	$0.53 \pm 0.04 \pm 0.01$	$0.38 \pm 0.03 \pm 0.01$		
$21 - 22$					
$22 - 23$	$0.46 \pm 0.05 \pm 0.01$	$0.20 \pm 0.03 \pm 0.01$	$0.25 \pm 0.03 \pm 0.01$	$0.33 \pm 0.04 \pm 0.01$	
$23 - 24$					
$24 - 25$	$0.23 \pm 0.04 \pm 0.01$	$0.25 \pm 0.03 \pm 0.01$	$0.11 \pm 0.02 \pm 0.01$		
$25 - 26$					
$26 - 27$	$0.31 \pm 0.05 \pm 0.01$	$0.14 \pm 0.02 \pm 0.01$	$0.15 \pm 0.03 \pm 0.02$		
$27 - 28$					
$28 - 29$		$0.09 \pm 0.02 \pm 0.01$			
$29 - 30$					

Table 6: Production cross-section $\sigma_{\rm bin}^{\Upsilon(1S)\to\mu^+\mu^-}$ [pb] in $(p_{\rm T}, y)$ bins for $\sqrt{s} = 8\,\text{TeV}$. The first uncertainties are statistical and the second are the uncorrelated component of the systematic uncertainties. The overall correlated systematic uncertainty is 2.8% and is not included in the numbers in the table. The horizontal lines indicate bin boundaries.

$p_{\rm T}$ [GeV/c]	$2.0 < y < 2.5$	$2.5 < y < 3.0$	$3.0 < y < 3.5$	$3.5 < y < 4.0$	$4.0 < y < 4.5$
$0 - 1$	$38.5 \pm 0.5 \pm 0.6$	$37.2 \pm 0.3 \pm 0.3$	$32.7 \pm 0.2 \pm 0.3$	$26.28 \pm 0.22 \pm 0.12$	$15.8 \pm 0.3 \pm 0.2$
$1 - 2$	$98.4 \pm 0.8 \pm 0.5$	$94.3 \pm 0.4 \pm 0.3$	$81.5 \pm 0.4 \pm 0.4$	$65.7 \pm 0.4 \pm 0.7$	$39.6 \pm 0.5 \pm 0.4$
$2 - 3$	$124.9 \pm 0.8 \pm 0.8$	$122.1 \pm 0.5 \pm 0.7$	$103.7 \pm 0.4 \pm 0.8$	$80.9 \pm 0.4 \pm 0.2$	$48.0 \pm 0.5 \pm 0.3$
$3 - 4$	$127.3 \pm 0.8 \pm 0.9$	$122.4 \pm 0.5 \pm 0.3$	$101.9 \pm 0.4 \pm 0.6$	$79.4 \pm 0.4 \pm 0.5$	$45.8 \pm 0.5 \pm 0.3$
$4 - 5$	$114.7 \pm 0.8 \pm 0.5$	$107.1 \pm 0.4 \pm 0.3$	$88.7 \pm 0.4 \pm 0.3$	$69.2 \pm 0.4 \pm 0.3$	$38.4 \pm 0.4 \pm 0.6$
$5 - 6$	$93.7 \pm 0.7 \pm 0.7$	$88.6 \pm 0.4 \pm 0.5$	$72.7 \pm 0.3 \pm 0.5$	$54.7 \pm 0.3 \pm 0.5$	$31.4 \pm 0.4 \pm 0.1$
$6 - 7$	$74.1 \pm 0.6 \pm 0.8$	$69.1 \pm 0.4 \pm 0.3$	$56.0 \pm 0.3 \pm 0.3$	$42.0 \pm 0.3 \pm 0.4$	$23.20 \pm 0.33 \pm 0.08$
$7 - 8$	$56.7 \pm 0.5 \pm 0.5$	$52.7 \pm 0.3 \pm 0.3$	$42.8 \pm 0.2 \pm 0.2$	$31.48 \pm 0.24 \pm 0.16$	$17.65 \pm 0.29 \pm 0.15$
$8 - 9$	$42.9 \pm 0.5 \pm 0.3$	$39.9 \pm 0.3 \pm 0.3$	$31.41 \pm 0.21 \pm 0.13$	$23.19 \pm 0.20 \pm 0.04$	$11.86 \pm 0.24 \pm 0.19$
$9 - 10$	$32.6 \pm 0.4 \pm 0.3$	$30.04 \pm 0.23 \pm 0.14$	$23.53 \pm 0.18 \pm 0.07$	$16.36 \pm 0.17 \pm 0.14$	$7.87 \pm 0.20 \pm 0.05$
$10 - 11$	$25.1 \pm 0.4 \pm 0.4$	$22.10 \pm 0.19 \pm 0.25$	$17.17 \pm 0.15 \pm 0.07$	$11.85 \pm 0.14 \pm 0.14$	$5.02 \pm 0.17 \pm 0.13$
$11 - 12$	$18.6 \pm 0.3 \pm 0.2$	$16.32 \pm 0.16 \pm 0.12$	$12.62 \pm 0.13 \pm 0.14$	$8.87 \pm 0.12 \pm 0.06$	$3.23 \pm 0.14 \pm 0.05$
$12 - 13$	$13.77 \pm 0.25 \pm 0.12$	$12.00 \pm 0.14 \pm 0.12$	$9.05 \pm 0.11 \pm 0.05$	$6.32 \pm 0.10 \pm 0.06$	$2.41 \pm 0.14 \pm 0.05$
$13 - 14$	$10.24 \pm 0.22 \pm 0.13$	$9.09 \pm 0.12 \pm 0.08$	$6.70 \pm 0.09 \pm 0.09$	$4.49 \pm 0.09 \pm 0.05$	$2.46 \pm 0.15 \pm 0.07$
$14 - 15$	$7.89 \pm 0.19 \pm 0.17$	$6.71 \pm 0.10 \pm 0.06$	$4.93 \pm 0.08 \pm 0.01$	$3.24 \pm 0.07 \pm 0.07$	
$15 - 16$	$5.90 \pm 0.16 \pm 0.09$	$5.15 \pm 0.09 \pm 0.04$	$3.64 \pm 0.07 \pm 0.03$	$2.27 \pm 0.06 \pm 0.02$	
$16 - 17$	$4.37 \pm 0.13 \pm 0.02$	$3.68 \pm 0.07 \pm 0.03$	$2.79 \pm 0.06 \pm 0.01$	$1.79 \pm 0.06 \pm 0.03$	
$17 - 18$	$3.35 \pm 0.12 \pm 0.05$	$2.83 \pm 0.06 \pm 0.01$	$1.96 \pm 0.05 \pm 0.02$	$1.25 \pm 0.05 \pm 0.02$	$1.75 \pm 0.15 \pm 0.05$
$18 - 19$	$2.78 \pm 0.10 \pm 0.03$	$2.10 \pm 0.05 \pm 0.01$	$1.55 \pm 0.05 \pm 0.01$	$0.91 \pm 0.04 \pm 0.03$	
$19 - 20$	$2.02 \pm 0.09 \pm 0.01$	$1.67 \pm 0.05 \pm 0.01$	$1.26 \pm 0.04 \pm 0.02$	$0.75 \pm 0.04 \pm 0.01$	
$20 - 21$	$2.72 \pm 0.10 \pm 0.02$	$2.34 \pm 0.06 \pm 0.03$	$1.69 \pm 0.05 \pm 0.03$	$1.29 \pm 0.05 \pm 0.02$	
$21 - 22$					
$22 - 23$	$1.66 \pm 0.08 \pm 0.01$	$1.38 \pm 0.04 \pm 0.01$	$0.93 \pm 0.04 \pm 0.01$		
$23 - 24$					
$24 - 25$	$1.24 \pm 0.07 \pm 0.02$	$0.86 \pm 0.04 \pm 0.02$	$0.56 \pm 0.03 \pm 0.01$		
$25 - 26$					
$26 - 27$	$1.20 \pm 0.07 \pm 0.02$	$0.56 \pm 0.03 \pm 0.01$	$0.61 \pm 0.03 \pm 0.01$		
$27 - 28$					
$28 - 29$		$0.39 \pm 0.03 \pm 0.01$			
$29 - 30$					

Table 7: Production cross-section $\sigma_{\rm bin}^{\Upsilon(2S)\to\mu^+\mu^-}$ [pb] in $(p_{\rm T}, y)$ bins for $\sqrt{s} = 8\,\text{TeV}$. The first uncertainties are statistical and the second are the uncorrelated component of the systematic uncertainties. The overall correlated systematic uncertainty is 2.8% and is not included in the numbers in the table. The horizontal lines indicate bin boundaries.

$p_{\rm T}$ [GeV/c]	$2.0 < y < 2.5$	$2.5 < y < 3.0$	$3.0 < y < 3.5$	$3.5 < y < 4.0$	$4.0 < y < 4.5$
$0 - 1$	$8.11 \pm 0.24 \pm 0.22$	$7.90 \pm 0.13 \pm 0.13$	$7.07 \pm 0.12 \pm 0.09$	$5.58 \pm 0.11 \pm 0.05$	$3.53 \pm 0.15 \pm 0.07$
$1 - 2$	$21.8 \pm 0.4 \pm 0.2$	$20.44 \pm 0.22 \pm 0.09$	$17.55 \pm 0.19 \pm 0.12$	$14.30 \pm 0.18 \pm 0.22$	$8.23 \pm 0.24 \pm 0.18$
$2 - 3$	$27.7 \pm 0.4 \pm 0.2$	$26.53 \pm 0.25 \pm 0.23$	$22.55 \pm 0.21 \pm 0.24$	$17.80 \pm 0.20 \pm 0.08$	$10.83 \pm 0.26 \pm 0.10$
$3 - 4$	$29.9 \pm 0.4 \pm 0.4$	$28.24 \pm 0.26 \pm 0.12$	$23.24 \pm 0.21 \pm 0.27$	$18.80 \pm 0.20 \pm 0.25$	$10.62 \pm 0.25 \pm 0.17$
$4 - 5$	$27.4 \pm 0.4 \pm 0.2$	$26.00 \pm 0.25 \pm 0.13$	$20.79 \pm 0.20 \pm 0.11$	$16.57 \pm 0.19 \pm 0.15$	$9.6 \pm 0.2 \pm 0.3$
$5 - 6$	$23.5 \pm 0.4 \pm 0.2$	$22.39 \pm 0.23 \pm 0.18$	$18.16 \pm 0.19 \pm 0.20$	$13.59 \pm 0.17 \pm 0.19$	$8.26 \pm 0.21 \pm 0.03$
$6 - 7$	$20.3 \pm 0.4 \pm 0.4$	$18.62 \pm 0.21 \pm 0.13$	$15.02 \pm 0.17 \pm 0.17$	$11.13 \pm 0.16 \pm 0.20$	$6.27 \pm 0.18 \pm 0.04$
$7 - 8$	$16.7 \pm 0.3 \pm 0.2$	$14.85 \pm 0.18 \pm 0.16$	$11.87 \pm 0.15 \pm 0.14$	$8.78 \pm 0.14 \pm 0.10$	$5.06 \pm 0.16 \pm 0.08$
$8 - 9$	$13.43 \pm 0.28 \pm 0.17$	$11.79 \pm 0.16 \pm 0.16$	$9.16 \pm 0.13 \pm 0.05$	$6.86 \pm 0.12 \pm 0.03$	$3.65 \pm 0.15 \pm 0.12$
$9 - 10$	$10.16 \pm 0.24 \pm 0.15$	$9.20 \pm 0.14 \pm 0.07$	$7.14 \pm 0.11 \pm 0.04$	$5.26 \pm 0.10 \pm 0.07$	$2.49 \pm 0.13 \pm 0.02$
$10 - 11$	$8.15 \pm 0.22 \pm 0.16$	$6.97 \pm 0.12 \pm 0.11$	$5.70 \pm 0.09 \pm 0.05$	$3.87 \pm 0.09 \pm 0.07$	$1.82 \pm 0.11 \pm 0.06$
$11 - 12$	$6.55 \pm 0.20 \pm 0.15$	$5.37 \pm 0.10 \pm 0.07$	$4.15 \pm 0.08 \pm 0.09$	$2.94 \pm 0.08 \pm 0.04$	$1.11 \pm 0.09 \pm 0.03$
$12 - 13$	$4.93 \pm 0.16 \pm 0.08$	$4.19 \pm 0.09 \pm 0.05$	$3.19 \pm 0.07 \pm 0.03$	$2.25 \pm 0.07 \pm 0.03$	$0.74 \pm 0.08 \pm 0.04$
$13 - 14$	$3.93 \pm 0.15 \pm 0.08$	$3.18 \pm 0.08 \pm 0.04$	$2.45 \pm 0.06 \pm 0.06$	$1.66 \pm 0.06 \pm 0.03$	$0.84 \pm 0.09 \pm 0.04$
$14 - 15$	$2.99 \pm 0.13 \pm 0.10$	$2.48 \pm 0.07 \pm 0.04$	$1.83 \pm 0.05 \pm 0.01$	$1.27 \pm 0.05 \pm 0.05$	
$15 - 16$	$2.36 \pm 0.11 \pm 0.07$	$2.03 \pm 0.06 \pm 0.02$	$1.42 \pm 0.05 \pm 0.03$	$0.92 \pm 0.04 \pm 0.01$	
$16 - 17$	$1.89 \pm 0.10 \pm 0.02$	$1.48 \pm 0.05 \pm 0.02$	$1.09 \pm 0.04 \pm 0.01$	$0.68 \pm 0.04 \pm 0.03$	
$17 - 18$	$1.31 \pm 0.08 \pm 0.03$	$1.19 \pm 0.04 \pm 0.01$	$0.86 \pm 0.04 \pm 0.01$	$0.52 \pm 0.04 \pm 0.01$	$0.79 \pm 0.11 \pm 0.03$
$18 - 19$	$1.15 \pm 0.07 \pm 0.02$	$0.92 \pm 0.04 \pm 0.01$	$0.69 \pm 0.03 \pm 0.01$	$0.39 \pm 0.03 \pm 0.02$	
$19 - 20$	$0.89 \pm 0.06 \pm 0.01$	$0.70 \pm 0.03 \pm 0.01$	$0.46 \pm 0.03 \pm 0.01$	$0.32 \pm 0.02 \pm 0.01$	
$20 - 21$	$1.34 \pm 0.08 \pm 0.01$	$1.08 \pm 0.04 \pm 0.02$	$0.69 \pm 0.03 \pm 0.02$	$0.59 \pm 0.04 \pm 0.02$	
$21 - 22$					
$22 - 23$	$0.76 \pm 0.06 \pm 0.01$	$0.64 \pm 0.03 \pm 0.01$	$0.41 \pm 0.03 \pm 0.01$		
$23 - 24$					
$24 - 25$	$0.63 \pm 0.05 \pm 0.01$	$0.41 \pm 0.03 \pm 0.01$	$0.28 \pm 0.02 \pm 0.01$		
$25 - 26$					
$26 - 27$	$0.55 \pm 0.05 \pm 0.02$	$0.29 \pm 0.02 \pm 0.01$	$0.27 \pm 0.02 \pm 0.01$		
$27 - 28$					
$28 - 29$		$0.19 \pm 0.02 \pm 0.01$			
$29 - 30$					

Table 8: Production cross-section $\sigma_{\rm bin}^{\Upsilon(3S)\to\mu^+\mu^-}$ [pb] in $(p_{\rm T}, y)$ bins for $\sqrt{s} = 8\,\text{TeV}$. The first uncertainties are statistical and the second are the uncorrelated component of the systematic uncertainty. The overall correlated systematic uncertainty is 2.8% and is not included in the numbers in the table. The horizontal lines indicate the bin boundaries.

$p_{\rm T}$ [GeV/c]	$2.0 < y < 2.5$	$2.5 < y < 3.0$	$3.0 < y < 3.5$	$3.5 < y < 4.0$	$4.0 < y < 4.5$
$0 - 1$	$3.30 \pm 0.17 \pm 0.09$	$3.29 \pm 0.10 \pm 0.04$	$2.72 \pm 0.09 \pm 0.05$	$2.42 \pm 0.08 \pm 0.02$	$1.47 \pm 0.11 \pm 0.03$
$1 - 2$	$8.19 \pm 0.27 \pm 0.01$	$8.45 \pm 0.16 \pm 0.06$	$7.18 \pm 0.14 \pm 0.02$	$5.83 \pm 0.13 \pm 0.13$	$3.43 \pm 0.17 \pm 0.11$
$2 - 3$	$10.73 \pm 0.30 \pm 0.14$	$11.16 \pm 0.18 \pm 0.07$	$9.05 \pm 0.15 \pm 0.14$	$7.56 \pm 0.14 \pm 0.03$	$4.94 \pm 0.19 \pm 0.05$
$3 - 4$	$12.44 \pm 0.31 \pm 0.07$	$12.00 \pm 0.18 \pm 0.04$	$9.99 \pm 0.16 \pm 0.08$	$7.98 \pm 0.15 \pm 0.10$	$4.69 \pm 0.18 \pm 0.08$
$4 - 5$	$11.37 \pm 0.30 \pm 0.07$	$11.42 \pm 0.18 \pm 0.01$	$9.51 \pm 0.15 \pm 0.05$	$7.70 \pm 0.14 \pm 0.05$	$4.48 \pm 0.17 \pm 0.20$
$5 - 6$	$10.06 \pm 0.27 \pm 0.04$	$10.21 \pm 0.17 \pm 0.07$	$8.53 \pm 0.14 \pm 0.09$	$6.64 \pm 0.13 \pm 0.12$	$3.68 \pm 0.15 \pm 0.01$
$6 - 7$	$9.35 \pm 0.26 \pm 0.16$	$8.60 \pm 0.15 \pm 0.03$	$7.36 \pm 0.13 \pm 0.07$	$5.66 \pm 0.12 \pm 0.12$	$3.13 \pm 0.14 \pm 0.01$
$7 - 8$	$7.83 \pm 0.23 \pm 0.06$	$7.48 \pm 0.14 \pm 0.05$	$6.14 \pm 0.11 \pm 0.08$	$4.79 \pm 0.11 \pm 0.04$	$2.48 \pm 0.12 \pm 0.04$
$8 - 9$	$6.66 \pm 0.21 \pm 0.05$	$6.13 \pm 0.12 \pm 0.08$	$4.91 \pm 0.10 \pm 0.03$	$3.64 \pm 0.09 \pm 0.01$	$1.75 \pm 0.11 \pm 0.05$
$9 - 10$	$5.29 \pm 0.19 \pm 0.07$	$4.81 \pm 0.11 \pm 0.04$	$3.99 \pm 0.09 \pm 0.02$	$3.00 \pm 0.08 \pm 0.05$	$1.24 \pm 0.09 \pm 0.01$
$10 - 11$	$4.11 \pm 0.17 \pm 0.08$	$3.98 \pm 0.09 \pm 0.08$	$3.19 \pm 0.07 \pm 0.03$	$2.42 \pm 0.07 \pm 0.05$	$1.10 \pm 0.09 \pm 0.07$
$11 - 12$	$3.27 \pm 0.15 \pm 0.09$	$3.16 \pm 0.08 \pm 0.04$	$2.49 \pm 0.06 \pm 0.07$	$1.73 \pm 0.06 \pm 0.02$	$0.69 \pm 0.07 \pm 0.02$
$12 - 13$	$2.91 \pm 0.13 \pm 0.04$	$2.65 \pm 0.07 \pm 0.04$	$1.95 \pm 0.06 \pm 0.02$	$1.41 \pm 0.06 \pm 0.02$	$0.46 \pm 0.07 \pm 0.01$
$13 - 14$	$2.41 \pm 0.12 \pm 0.04$	$2.07 \pm 0.06 \pm 0.03$	$1.52 \pm 0.05 \pm 0.04$	$1.05 \pm 0.05 \pm 0.02$	$0.60 \pm 0.09 \pm 0.02$
$14 - 15$	$1.93 \pm 0.11 \pm 0.07$	$1.67 \pm 0.06 \pm 0.04$	$1.17 \pm 0.04 \pm 0.01$	$0.83 \pm 0.04 \pm 0.03$	
$15 - 16$	$1.52 \pm 0.09 \pm 0.04$	$1.21 \pm 0.05 \pm 0.02$	$0.90 \pm 0.04 \pm 0.02$	$0.61 \pm 0.04 \pm 0.01$	
$16 - 17$	$1.10 \pm 0.08 \pm 0.02$	$0.97 \pm 0.04 \pm 0.01$	$0.76 \pm 0.04 \pm 0.01$	$0.42 \pm 0.03 \pm 0.02$	
$17 - 18$	$0.89 \pm 0.07 \pm 0.02$	$0.77 \pm 0.04 \pm 0.01$	$0.56 \pm 0.03 \pm 0.01$	$0.40 \pm 0.032 \pm 0.01$	$0.46 \pm 0.08 \pm 0.01$
$18 - 19$	$0.79 \pm 0.06 \pm 0.01$	$0.58 \pm 0.03 \pm 0.01$	$0.43 \pm 0.03 \pm 0.01$	$0.31 \pm 0.029 \pm 0.01$	
$19 - 20$	$0.59 \pm 0.05 \pm 0.01$	$0.49 \pm 0.03 \pm 0.01$	$0.32 \pm 0.02 \pm 0.01$	$0.20 \pm 0.02 \pm 0.01$	
$20 - 21$	$0.84 \pm 0.06 \pm 0.01$	$0.73 \pm 0.04 \pm 0.02$	$0.46 \pm 0.03 \pm 0.01$	$0.46 \pm 0.04 \pm 0.02$	
$21 - 22$					
$22 - 23$	$0.51 \pm 0.05 \pm 0.01$	$0.46 \pm 0.03 \pm 0.04$	$0.32 \pm 0.02 \pm 0.01$		
$23 - 24$					
$24 - 25$	$0.34 \pm 0.04 \pm 0.01$	$0.30 \pm 0.02 \pm 0.01$	$0.21 \pm 0.03 \pm 0.01$		
$25 - 26$					
$26 - 27$	$0.52 \pm 0.05 \pm 0.02$	$0.18 \pm 0.02 \pm 0.01$	$0.20 \pm 0.02 \pm 0.01$		
$27 - 28$					
$28 - 29$		$0.12 \pm 0.02 \pm 0.01$			
$29 - 30$					

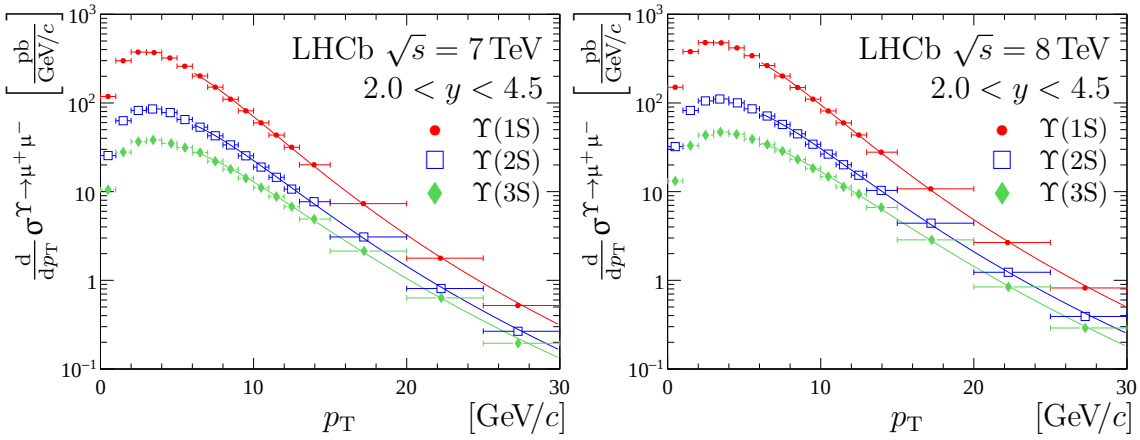

Figure 3: Differential cross-sections $\frac{\mathrm{d}}{\mathrm{d}p_\mathrm{T}}\sigma^{\Upsilon\to\mu^+\mu^-}$ in the range $2.0 < y < 4.5$ for (red solid circles) $\Upsilon(1S)$, (blue open squares) $\Upsilon(2S)$ and (green solid diamonds) $\Upsilon(3S)$ mesons for (left) $\sqrt{s} = 7\,\mathrm{TeV}$ and (right) $\sqrt{s} = 8\,\mathrm{TeV}$ data. The curves show the fit results with the Tsallis function in the range $6 < p_\mathrm{T} < 30\,\mathrm{GeV}/c$. The data points are positioned in the bins according to Eq. (6) in Ref. [61].

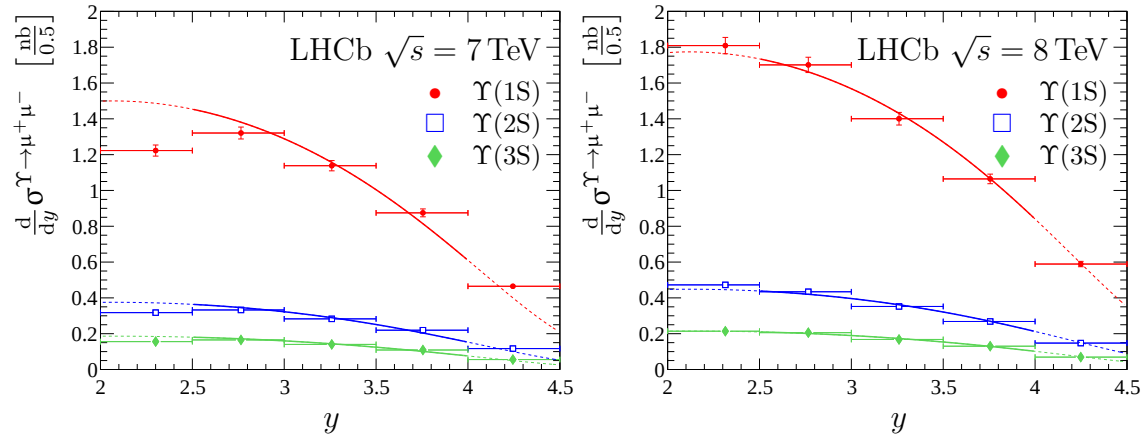

Figure 4: Differential cross-sections $\frac{\mathrm{d}}{\mathrm{d}y}\sigma^{\Upsilon\to\mu^+\mu^-}$ in the range $p_\mathrm{T} < 30\,\mathrm{GeV}/c$ for (red solid circles) $\Upsilon(1S)$, (blue open squares) $\Upsilon(2S)$ and (green solid diamonds) $\Upsilon(3S)$ mesons for (left) $\sqrt{s} = 7\,\mathrm{TeV}$ and (right) $\sqrt{s} = 8\,\mathrm{TeV}$ data. Thick lines show fit results with the CO model predictions from Ref. [62,63] in the region $2.5 < y < 4.0$, and dashed lines show the extrapolation to the full region $2.0 < y < 4.5$. The data points are positioned in the bins according to Eq. (6) in Ref. [61].

The ratios of integrated production cross-section $\mathscr{R}_{8/7}$ are presented in Table 11 for the full ($p_\mathrm{T} < 30\,\mathrm{GeV}/c$) and reduced ($p_\mathrm{T} < 15\,\mathrm{GeV}/c$) ranges. The results for the reduced range are consistent with the previous measurements, confirming the increase of the bottomonium production cross-section of approximately 30% when the centre-of-mass energy

Table 9: Results of the fits to the transverse momentum spectra of Υ mesons using the Tsallis function in the reduced range $6 < p_{\rm T} < 30\,{\rm GeV}/c$.

	$\sqrt{s}$	T [GeV]	n
Υ(1S)	7 TeV	1.19 ± 0.04	8.01 ± 0.33
	8 TeV	1.20 ± 0.04	7.71 ± 0.27
Υ(2S)	7 TeV	1.33 ± 0.05	7.57 ± 0.41
	8 TeV	1.37 ± 0.05	7.53 ± 0.34
Υ(3S)	7 TeV	1.53 ± 0.07	7.85 ± 0.56
	8 TeV	1.63 ± 0.06	8.23 ± 0.51

Table 10: The production cross-section $\sigma^{\Upsilon\to\mu^+\mu^-}$ (in pb) for Υ mesons in the full kinematic range $p_{\rm T} < 30\,{\rm GeV}/c$ (left two columns), and reduced range $p_{\rm T} < 15\,{\rm GeV}/c$ (right two columns), for $2.0 < y < 4.5$. The first uncertainties are statistical and the second systematic.

	$p_{\rm T} < 30\,{\rm GeV}/c$		$p_{\rm T} < 15\,{\rm GeV}/c$	
	$\sqrt{s} = 7\,{\rm TeV}$	$\sqrt{s} = 8\,{\rm TeV}$	$\sqrt{s} = 7\,{\rm TeV}$	$\sqrt{s} = 8\,{\rm TeV}$
$\sigma^{\Upsilon(1S)\to\mu^+\mu^-}$	$2510 \pm 3 \pm 80$	$3280 \pm 3 \pm 100$	$2460 \pm 3 \pm 80$	$3210 \pm 3 \pm 90$
$\sigma^{\Upsilon(2S)\to\mu^+\mu^-}$	$635 \pm 2 \pm 20$	$837 \pm 2 \pm 25$	$614 \pm 2 \pm 20$	$807 \pm 2 \pm 24$
$\sigma^{\Upsilon(3S)\to\mu^+\mu^-}$	$313 \pm 2 \pm 10$	$393 \pm 1 \pm 12$	$298 \pm 1 \pm 10$	$373 \pm 1 \pm 11$

increases from $\sqrt{s} = 7$ to 8 TeV [22, 23].

The ratios $\mathscr{R}_{8/7}$ as a function of $p_{\rm T}$ integrated over the region $2.0 < y < 4.5$ are shown in Fig. 5a. The ratios are fitted with a linear function. The fit quality is good, with a p-value exceeding 35% for all cases, and the slopes are found to be 10.8 ± 0.6, 9.5 ± 1.2 and 9.8 ± 1.6 (in units of $10^{-3}/\,({\rm GeV}/c)$) for Υ(1S), Υ(2S) and Υ(3S), respectively. The measurements are compared with the NRQCD theory predictions [11] in the same kinematic range, where only uncertainties from the CO long distance matrix elements are considered since most other uncertainties are expected to cancel in the ratio. The theory predictions are independent on the Υ state and are consistently lower than the measurements.

The ratio $\mathscr{R}_{8/7}$ as a function of rapidity, integrated over the region $p_{\rm T} < 30\,{\rm GeV}/c$ is shown in Fig. 5b. The ratios are compared with the expectations from the CO mechanism [62, 63] with normalisation factors fixed from the fits of Fig. 4. The trend observed in data does not agree with the pure CO model. It can be noted that also for open beauty hadrons the differential cross-sections exhibit a larger rise as a function of $\sqrt{s}$ at smaller rapidities [54], while the FONLL calculations [64] predict this behaviour towards larger rapidity.

The ratios $\mathscr{R}_{\rm i,j}$ at $\sqrt{s} = 7$ and 8 TeV are reported in Fig. 6 and Tables 12, 13, 14 and 15

Table 11: The ratio of production cross-sections for Υ mesons at $\sqrt{s} = 8$ to that at $\sqrt{s} = 7\,\text{TeV}$ in the full kinematic range $p_{\rm T} < 30\,\text{GeV}/c$ (left) and reduced range $p_{\rm T} < 15\,\text{GeV}/c$ (right) for $2.0 < y < 4.5$. The first uncertainties are statistical and the second systematic.

	$p_{\rm T} < 30\,\text{GeV}/c$	$p_{\rm T} < 15\,\text{GeV}/c$
$\Upsilon(1S)$	$1.307 \pm 0.002 \pm 0.025$	$1.304 \pm 0.002 \pm 0.024$
$\Upsilon(2S)$	$1.319 \pm 0.005 \pm 0.025$	$1.315 \pm 0.005 \pm 0.024$
$\Upsilon(3S)$	$1.258 \pm 0.007 \pm 0.024$	$1.254 \pm 0.007 \pm 0.023$

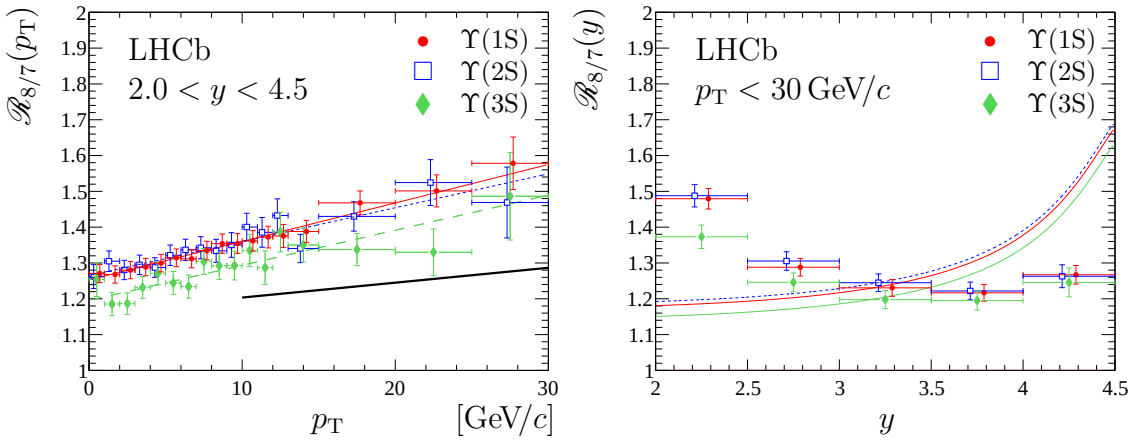

Figure 5: Ratios of the differential cross-sections (left) $\frac{\rm d}{{\rm d}p_{\rm T}}\sigma^{\Upsilon\to\mu^+\mu^-}$ and (right) $\frac{\rm d}{{\rm d}y}\sigma^{\Upsilon\to\mu^+\mu^-}$ at $\sqrt{s} = 8$ and 7 TeV for (red solid circles) $\Upsilon(1S)$, (blue open squares) $\Upsilon(2S)$ and (green solid diamonds) $\Upsilon(3S)$. On the left hand plot, the results of the fit with a linear function are shown with straight thin red solid, blue dotted and green dashed lines. In the same plot, the next-to-leading order NRQCD theory predictions [11] are shown as a thick line. On the right hand plot, the curved red solid, blue dotted and greed dashed lines show the CO model predictions [62, 63] with the normalisation fixed from the fits in Fig. 4 for $\Upsilon(1S)$, $\Upsilon(2S)$ and $\Upsilon(3S)$ mesons, respectively. Some data points are displaced from the bin centres to improve visibility.

as a function of $p_{\rm T}$ for different rapidity bins. The same ratios as a function of $p_{\rm T}$ integrated over rapidity, and as a function of y integrated over $p_{\rm T}$, are shown in Fig. 7. The ratios $\mathscr{R}_{\rm i,j}$ show little dependence on rapidity and increase as a function of $p_{\rm T}$, in agreement with previous observations by LHCb [22, 23], ATLAS [25] and CMS [26] at $\sqrt{s} = 7\,\text{TeV}$. The ratios of integrated cross-sections $\mathscr{R}_{\rm i,j}$ at $\sqrt{s} = 7$ and 8 TeV are reported in Table 16, for the full and the reduced $p_{\rm T}$ kinematic regions. All ratios $\mathscr{R}_{\rm i,j}$ agree with previous LHCb measurements. The ratio $\mathscr{R}_{2,1}$ agrees with the estimates of 0.27 from Refs. [63, 65], while $\mathscr{R}_{3,1}$ significantly exceeds the expected value of 0.04 [63, 65] but agrees with the range $0.14 - 0.22$, expected for the hypothesis of a large admixture of a hybrid quarkonium state in the $\Upsilon(3S)$ meson state [65].

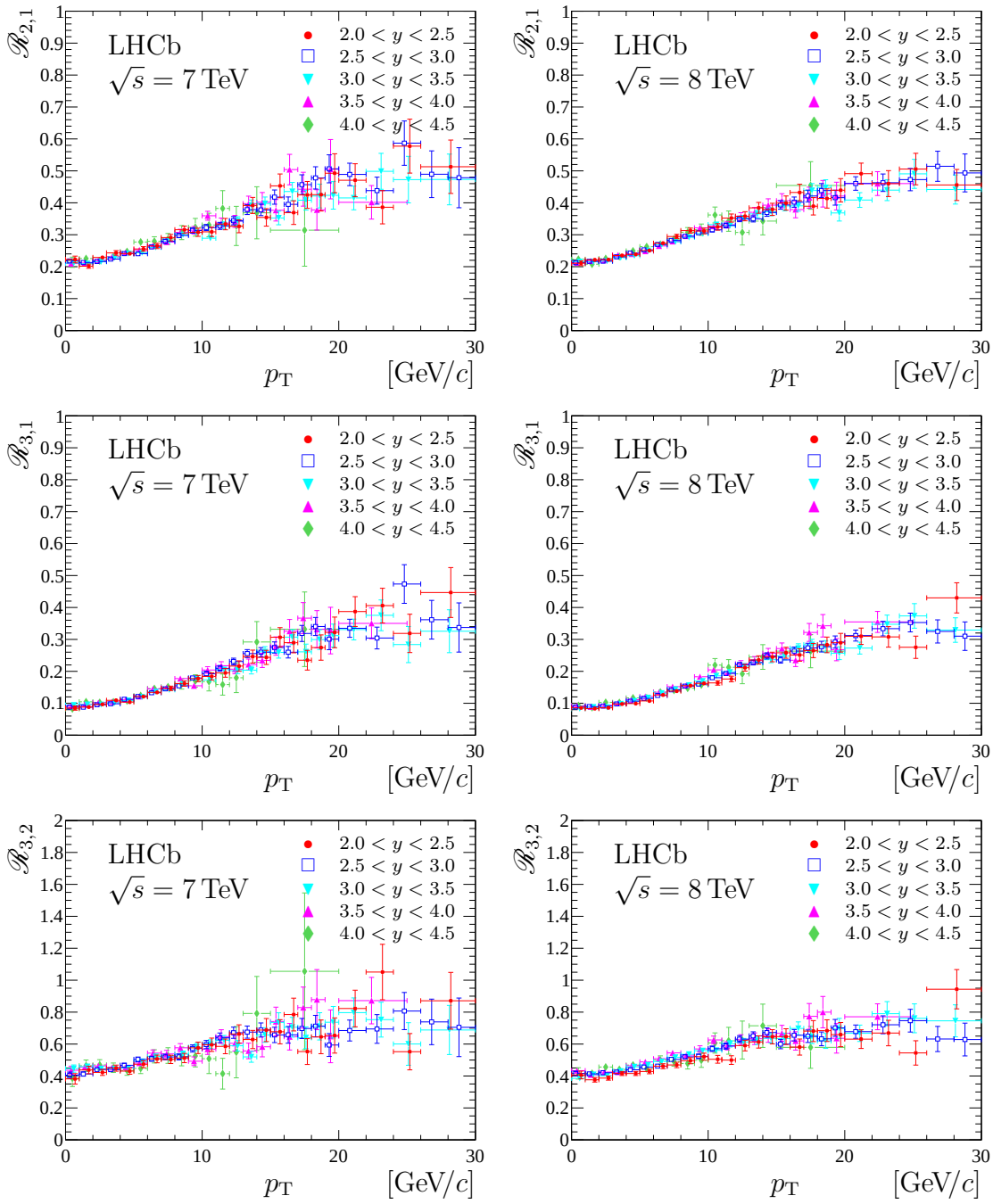

Figure 6: The production ratios $\mathscr{R}_{i,j}$ for (top) $\Upsilon(2S)$ to $\Upsilon(1S)$, (middle) $\Upsilon(3S)$ to $\Upsilon(1S)$, and (bottom) $\Upsilon(3S)$ to $\Upsilon(2S)$, measured with data collected at (left) $\sqrt{s} = 7\,\text{TeV}$ and (right) $\sqrt{s} = 8\,\text{TeV}$. The error bars indicate the sum in quadrature of the statistical and systematic uncertainties. The rapidity ranges $2.0 < y < 2.5$, $2.5 \leq y < 3.0$, $3.0 \leq y < 3.5$, $3.5 \leq y < 4.0$ and $4.0 \leq y < 4.5$ are shown with red circles, blue squares, cyan downward triangles, magenta upward triangles and green diamonds, respectively. Some data points are displaced from the bin centres to improve visibility.

Table 12: The ratio $\mathscr{R}_{2,1}$ for $\sqrt{s} = 7\,\text{TeV}$. The first uncertainties are statistical and the second are the uncorrelated component of the systematic uncertainties. The overall correlated systematic uncertainty is 0.7% and is not included in the numbers in the table. The horizontal lines indicate bin boundaries.

p_{T} [GeV/c]	$2.0 < y < 2.5$	$2.5 < y < 3.0$	$3.0 < y < 3.5$	$3.5 < y < 4.0$	$4.0 < y < 4.5$
$0 - 1$	$0.223 \pm 0.010 \pm 0.002$	$0.218 \pm 0.006 \pm 0.001$	$0.211 \pm 0.006 \pm 0.001$	$0.210 \pm 0.007 \pm 0.004$	$0.214 \pm 0.015 \pm 0.005$
$1 - 2$	$0.202 \pm 0.006 \pm 0.002$	$0.213 \pm 0.004 \pm 0.001$	$0.209 \pm 0.004 \pm 0.001$	$0.212 \pm 0.004 \pm 0.001$	$0.225 \pm 0.010 \pm 0.001$
$2 - 3$	$0.229 \pm 0.006 \pm 0.001$	$0.216 \pm 0.003 \pm 0.001$	$0.215 \pm 0.003 \pm 0.001$	$0.220 \pm 0.004 \pm 0.001$	$0.218 \pm 0.009 \pm 0.004$
$3 - 4$	$0.243 \pm 0.006 \pm 0.004$	$0.224 \pm 0.003 \pm 0.001$	$0.228 \pm 0.003 \pm 0.001$	$0.231 \pm 0.004 \pm 0.001$	$0.231 \pm 0.009 \pm 0.001$
$4 - 5$	$0.241 \pm 0.006 \pm 0.001$	$0.241 \pm 0.004 \pm 0.001$	$0.241 \pm 0.004 \pm 0.001$	$0.245 \pm 0.004 \pm 0.003$	$0.247 \pm 0.010 \pm 0.002$
$5 - 6$	$0.255 \pm 0.007 \pm 0.002$	$0.241 \pm 0.004 \pm 0.001$	$0.244 \pm 0.004 \pm 0.001$	$0.252 \pm 0.005 \pm 0.001$	$0.277 \pm 0.012 \pm 0.001$
$6 - 7$	$0.265 \pm 0.008 \pm 0.003$	$0.262 \pm 0.005 \pm 0.001$	$0.260 \pm 0.005 \pm 0.002$	$0.267 \pm 0.006 \pm 0.001$	$0.279 \pm 0.014 \pm 0.004$
$7 - 8$	$0.291 \pm 0.009 \pm 0.003$	$0.279 \pm 0.006 \pm 0.002$	$0.280 \pm 0.006 \pm 0.002$	$0.277 \pm 0.007 \pm 0.003$	$0.287 \pm 0.017 \pm 0.003$
$8 - 9$	$0.316 \pm 0.011 \pm 0.002$	$0.298 \pm 0.007 \pm 0.001$	$0.300 \pm 0.007 \pm 0.002$	$0.308 \pm 0.009 \pm 0.002$	$0.307 \pm 0.021 \pm 0.005$
$9 - 10$	$0.308 \pm 0.012 \pm 0.002$	$0.313 \pm 0.008 \pm 0.001$	$0.307 \pm 0.008 \pm 0.003$	$0.314 \pm 0.011 \pm 0.004$	$0.323 \pm 0.028 \pm 0.002$
$10 - 11$	$0.309 \pm 0.014 \pm 0.003$	$0.323 \pm 0.009 \pm 0.002$	$0.289 \pm 0.009 \pm 0.001$	$0.359 \pm 0.014 \pm 0.001$	$0.33 \pm 0.04 \pm 0.01$
$11 - 12$	$0.333 \pm 0.017 \pm 0.004$	$0.328 \pm 0.011 \pm 0.003$	$0.329 \pm 0.011 \pm 0.001$	$0.337 \pm 0.015 \pm 0.002$	$0.38 \pm 0.06 \pm 0.01$
$12 - 13$	$0.326 \pm 0.019 \pm 0.005$	$0.344 \pm 0.013 \pm 0.002$	$0.343 \pm 0.013 \pm 0.001$	$0.342 \pm 0.019 \pm 0.001$	$0.33 \pm 0.06 \pm 0.01$
$13 - 14$	$0.392 \pm 0.025 \pm 0.005$	$0.379 \pm 0.015 \pm 0.001$	$0.392 \pm 0.017 \pm 0.001$	$0.397 \pm 0.023 \pm 0.002$	$0.37 \pm 0.08 \pm 0.01$
$14 - 15$	$0.354 \pm 0.026 \pm 0.007$	$0.378 \pm 0.017 \pm 0.003$	$0.398 \pm 0.020 \pm 0.005$	$0.402 \pm 0.030 \pm 0.006$	
$15 - 16$	$0.45 \pm 0.04 \pm 0.01$	$0.418 \pm 0.022 \pm 0.002$	$0.353 \pm 0.021 \pm 0.001$	$0.377 \pm 0.033 \pm 0.004$	
$16 - 17$	$0.37 \pm 0.04 \pm 0.01$	$0.395 \pm 0.023 \pm 0.004$	$0.435 \pm 0.028 \pm 0.001$	$0.50 \pm 0.05 \pm 0.01$	
$17 - 18$	$0.42 \pm 0.04 \pm 0.01$	$0.457 \pm 0.031 \pm 0.001$	$0.408 \pm 0.031 \pm 0.001$	$0.44 \pm 0.05 \pm 0.01$	$0.31 \pm 0.11 \pm 0.01$
$18 - 19$	$0.43 \pm 0.05 \pm 0.01$	$0.478 \pm 0.035 \pm 0.002$	$0.42 \pm 0.04 \pm 0.01$	$0.38 \pm 0.06 \pm 0.01$	
$19 - 20$	$0.49 \pm 0.06 \pm 0.01$	$0.51 \pm 0.04 \pm 0.01$	$0.42 \pm 0.04 \pm 0.01$	$0.51 \pm 0.09 \pm 0.01$	
$20 - 21$	$0.47 \pm 0.05 \pm 0.01$	$0.489 \pm 0.035 \pm 0.002$	$0.42 \pm 0.04 \pm 0.01$		
$21 - 22$					
$22 - 23$	$0.39 \pm 0.05 \pm 0.01$	$0.44 \pm 0.04 \pm 0.01$	$0.50 \pm 0.06 \pm 0.01$	$0.40 \pm 0.05 \pm 0.01$	
$23 - 24$					
$24 - 25$	$0.58 \pm 0.08 \pm 0.01$	$0.59 \pm 0.07 \pm 0.01$	$0.47 \pm 0.07 \pm 0.01$		
$25 - 26$					
$26 - 27$	$0.51 \pm 0.08 \pm 0.01$	$0.49 \pm 0.07 \pm 0.01$	$0.47 \pm 0.08 \pm 0.02$		
$27 - 28$					
$28 - 29$		$0.48 \pm 0.09 \pm 0.01$			
$29 - 30$					

Table 13: The ratio $\mathscr{R}_{3,1}$ for $\sqrt{s} = 7\,\text{TeV}$. The first uncertainties are statistical and the second are the uncorrelated component of the systematic uncertainties. The overall correlated systematic uncertainty is 0.7% and is not included in the numbers in the table. The horizontal lines indicate bin boundaries.

p_{T} [GeV/c]	$2.0 < y < 2.5$	$2.5 < y < 3.0$	$3.0 < y < 3.5$	$3.5 < y < 4.0$	$4.0 < y < 4.5$
$0 - 1$	$0.085 \pm 0.007 \pm 0.001$	$0.088 \pm 0.004 \pm 0.001$	$0.094 \pm 0.004 \pm 0.002$	$0.091 \pm 0.005 \pm 0.002$	$0.083 \pm 0.010 \pm 0.003$
$1 - 2$	$0.088 \pm 0.004 \pm 0.001$	$0.088 \pm 0.003 \pm 0.001$	$0.096 \pm 0.003 \pm 0.001$	$0.096 \pm 0.003 \pm 0.001$	$0.105 \pm 0.007 \pm 0.001$
$2 - 3$	$0.097 \pm 0.004 \pm 0.001$	$0.095 \pm 0.002 \pm 0.001$	$0.096 \pm 0.002 \pm 0.001$	$0.102 \pm 0.003 \pm 0.001$	$0.102 \pm 0.006 \pm 0.004$
$3 - 4$	$0.109 \pm 0.004 \pm 0.002$	$0.099 \pm 0.002 \pm 0.001$	$0.101 \pm 0.002 \pm 0.001$	$0.105 \pm 0.003 \pm 0.001$	$0.104 \pm 0.006 \pm 0.001$
$4 - 5$	$0.104 \pm 0.004 \pm 0.001$	$0.113 \pm 0.003 \pm 0.001$	$0.109 \pm 0.003 \pm 0.001$	$0.111 \pm 0.003 \pm 0.002$	$0.108 \pm 0.007 \pm 0.001$
$5 - 6$	$0.121 \pm 0.005 \pm 0.002$	$0.121 \pm 0.003 \pm 0.001$	$0.120 \pm 0.003 \pm 0.001$	$0.121 \pm 0.004 \pm 0.001$	$0.124 \pm 0.008 \pm 0.001$
$6 - 7$	$0.134 \pm 0.006 \pm 0.002$	$0.133 \pm 0.004 \pm 0.001$	$0.136 \pm 0.004 \pm 0.001$	$0.145 \pm 0.005 \pm 0.001$	$0.146 \pm 0.010 \pm 0.004$
$7 - 8$	$0.147 \pm 0.007 \pm 0.002$	$0.145 \pm 0.004 \pm 0.001$	$0.142 \pm 0.004 \pm 0.001$	$0.149 \pm 0.005 \pm 0.002$	$0.152 \pm 0.012 \pm 0.002$
$8 - 9$	$0.162 \pm 0.008 \pm 0.002$	$0.155 \pm 0.005 \pm 0.001$	$0.161 \pm 0.005 \pm 0.002$	$0.177 \pm 0.007 \pm 0.001$	$0.160 \pm 0.016 \pm 0.002$
$9 - 10$	$0.177 \pm 0.009 \pm 0.002$	$0.179 \pm 0.006 \pm 0.001$	$0.178 \pm 0.006 \pm 0.002$	$0.155 \pm 0.008 \pm 0.003$	$0.170 \pm 0.019 \pm 0.001$
$10 - 11$	$0.184 \pm 0.011 \pm 0.001$	$0.193 \pm 0.007 \pm 0.001$	$0.173 \pm 0.007 \pm 0.001$	$0.204 \pm 0.010 \pm 0.001$	$0.168 \pm 0.026 \pm 0.013$
$11 - 12$	$0.195 \pm 0.013 \pm 0.002$	$0.209 \pm 0.008 \pm 0.003$	$0.205 \pm 0.009 \pm 0.001$	$0.218 \pm 0.012 \pm 0.002$	$0.158 \pm 0.033 \pm 0.001$
$12 - 13$	$0.217 \pm 0.016 \pm 0.003$	$0.231 \pm 0.010 \pm 0.001$	$0.202 \pm 0.010 \pm 0.001$	$0.207 \pm 0.014 \pm 0.001$	$0.18 \pm 0.05 \pm 0.01$
$13 - 14$	$0.246 \pm 0.019 \pm 0.005$	$0.256 \pm 0.012 \pm 0.002$	$0.204 \pm 0.012 \pm 0.001$	$0.221 \pm 0.017 \pm 0.001$	$0.29 \pm 0.06 \pm 0.01$
$14 - 15$	$0.244 \pm 0.022 \pm 0.003$	$0.260 \pm 0.014 \pm 0.002$	$0.261 \pm 0.015 \pm 0.004$	$0.234 \pm 0.022 \pm 0.003$	
$15 - 16$	$0.307 \pm 0.030 \pm 0.002$	$0.275 \pm 0.017 \pm 0.001$	$0.259 \pm 0.018 \pm 0.001$	$0.279 \pm 0.028 \pm 0.003$	
$16 - 17$	$0.290 \pm 0.032 \pm 0.003$	$0.260 \pm 0.018 \pm 0.002$	$0.307 \pm 0.023 \pm 0.002$	$0.33 \pm 0.04 \pm 0.01$	
$17 - 18$	$0.235 \pm 0.031 \pm 0.002$	$0.319 \pm 0.025 \pm 0.002$	$0.261 \pm 0.024 \pm 0.002$	$0.37 \pm 0.05 \pm 0.01$	$0.33 \pm 0.12 \pm 0.01$
$18 - 19$	$0.27 \pm 0.04 \pm 0.01$	$0.340 \pm 0.028 \pm 0.001$	$0.300 \pm 0.031 \pm 0.001$	$0.33 \pm 0.06 \pm 0.01$	
$19 - 20$	$0.32 \pm 0.05 \pm 0.01$	$0.301 \pm 0.032 \pm 0.006$	$0.31 \pm 0.04 \pm 0.01$	$0.33 \pm 0.07 \pm 0.01$	
$20 - 21$	$0.39 \pm 0.05 \pm 0.01$	$0.335 \pm 0.028 \pm 0.002$	$0.331 \pm 0.032 \pm 0.002$	$0.35 \pm 0.05 \pm 0.01$	
$21 - 22$					
$22 - 23$	$0.41 \pm 0.05 \pm 0.01$	$0.304 \pm 0.034 \pm 0.002$	$0.38 \pm 0.05 \pm 0.01$		
$23 - 24$					
$24 - 25$	$0.32 \pm 0.06 \pm 0.01$	$0.47 \pm 0.06 \pm 0.01$	$0.28 \pm 0.06 \pm 0.01$		
$25 - 26$					
$26 - 27$	$0.45 \pm 0.08 \pm 0.01$	$0.36 \pm 0.06 \pm 0.01$	$0.33 \pm 0.06 \pm 0.02$		
$27 - 28$					
$28 - 29$		$0.34 \pm 0.08 \pm 0.01$			
$29 - 30$					

Table 14: The ratio $\mathscr{R}_{2,1}$ for $\sqrt{s} = 8\,\text{TeV}$. The first uncertainties are statistical and the second are the uncorrelated component of the systematic uncertainties. The overall correlated systematic uncertainty is 0.7% and is not included in the numbers in the table. The horizontal lines indicate bin boundaries.

p_T [GeV/c]	$2.0 < y < 2.5$	$2.5 < y < 3.0$	$3.0 < y < 3.5$	$3.5 < y < 4.0$	$4.0 < y < 4.5$
$0 - 1$	$0.211 \pm 0.007 \pm 0.003$	$0.213 \pm 0.004 \pm 0.002$	$0.216 \pm 0.004 \pm 0.001$	$0.212 \pm 0.005 \pm 0.001$	$0.223 \pm 0.010 \pm 0.002$
$1 - 2$	$0.221 \pm 0.004 \pm 0.001$	$0.217 \pm 0.003 \pm 0.001$	$0.215 \pm 0.003 \pm 0.001$	$0.218 \pm 0.003 \pm 0.001$	$0.208 \pm 0.006 \pm 0.003$
$2 - 3$	$0.222 \pm 0.004 \pm 0.001$	$0.217 \pm 0.002 \pm 0.001$	$0.218 \pm 0.002 \pm 0.001$	$0.220 \pm 0.003 \pm 0.001$	$0.225 \pm 0.006 \pm 0.001$
$3 - 4$	$0.235 \pm 0.004 \pm 0.001$	$0.231 \pm 0.002 \pm 0.001$	$0.228 \pm 0.002 \pm 0.001$	$0.237 \pm 0.003 \pm 0.002$	$0.232 \pm 0.006 \pm 0.002$
$4 - 5$	$0.238 \pm 0.004 \pm 0.001$	$0.243 \pm 0.003 \pm 0.001$	$0.234 \pm 0.002 \pm 0.001$	$0.240 \pm 0.003 \pm 0.001$	$0.249 \pm 0.007 \pm 0.005$
$5 - 6$	$0.251 \pm 0.005 \pm 0.001$	$0.253 \pm 0.003 \pm 0.001$	$0.250 \pm 0.003 \pm 0.001$	$0.249 \pm 0.003 \pm 0.002$	$0.263 \pm 0.007 \pm 0.001$
$6 - 7$	$0.274 \pm 0.005 \pm 0.003$	$0.270 \pm 0.003 \pm 0.001$	$0.268 \pm 0.003 \pm 0.002$	$0.265 \pm 0.004 \pm 0.002$	$0.270 \pm 0.009 \pm 0.001$
$7 - 8$	$0.294 \pm 0.006 \pm 0.002$	$0.282 \pm 0.004 \pm 0.002$	$0.278 \pm 0.004 \pm 0.002$	$0.279 \pm 0.005 \pm 0.002$	$0.287 \pm 0.010 \pm 0.002$
$8 - 9$	$0.313 \pm 0.007 \pm 0.002$	$0.295 \pm 0.004 \pm 0.002$	$0.292 \pm 0.004 \pm 0.001$	$0.296 \pm 0.006 \pm 0.001$	$0.308 \pm 0.014 \pm 0.006$
$9 - 10$	$0.312 \pm 0.008 \pm 0.002$	$0.306 \pm 0.005 \pm 0.001$	$0.304 \pm 0.005 \pm 0.001$	$0.322 \pm 0.007 \pm 0.002$	$0.316 \pm 0.018 \pm 0.001$
$10 - 11$	$0.324 \pm 0.010 \pm 0.002$	$0.315 \pm 0.006 \pm 0.002$	$0.332 \pm 0.006 \pm 0.002$	$0.327 \pm 0.008 \pm 0.003$	$0.362 \pm 0.025 \pm 0.004$
$11 - 12$	$0.352 \pm 0.012 \pm 0.004$	$0.329 \pm 0.007 \pm 0.002$	$0.328 \pm 0.007 \pm 0.004$	$0.331 \pm 0.010 \pm 0.003$	$0.343 \pm 0.032 \pm 0.004$
$12 - 13$	$0.358 \pm 0.014 \pm 0.004$	$0.350 \pm 0.008 \pm 0.002$	$0.352 \pm 0.009 \pm 0.001$	$0.357 \pm 0.012 \pm 0.002$	$0.31 \pm 0.04 \pm 0.01$
$13 - 14$	$0.384 \pm 0.016 \pm 0.003$	$0.350 \pm 0.009 \pm 0.001$	$0.365 \pm 0.010 \pm 0.004$	$0.370 \pm 0.015 \pm 0.002$	$0.34 \pm 0.04 \pm 0.01$
$14 - 15$	$0.379 \pm 0.018 \pm 0.005$	$0.370 \pm 0.011 \pm 0.003$	$0.372 \pm 0.012 \pm 0.001$	$0.393 \pm 0.018 \pm 0.008$	
$15 - 16$	$0.399 \pm 0.021 \pm 0.005$	$0.393 \pm 0.013 \pm 0.002$	$0.390 \pm 0.015 \pm 0.003$	$0.407 \pm 0.022 \pm 0.003$	
$16 - 17$	$0.432 \pm 0.025 \pm 0.002$	$0.402 \pm 0.016 \pm 0.002$	$0.390 \pm 0.017 \pm 0.002$	$0.379 \pm 0.024 \pm 0.008$	
$17 - 18$	$0.389 \pm 0.027 \pm 0.003$	$0.421 \pm 0.018 \pm 0.001$	$0.439 \pm 0.021 \pm 0.001$	$0.416 \pm 0.032 \pm 0.005$	$0.45 \pm 0.07 \pm 0.01$
$18 - 19$	$0.414 \pm 0.030 \pm 0.001$	$0.438 \pm 0.021 \pm 0.003$	$0.448 \pm 0.024 \pm 0.001$	$0.43 \pm 0.04 \pm 0.01$	
$19 - 20$	$0.44 \pm 0.04 \pm 0.01$	$0.416 \pm 0.023 \pm 0.001$	$0.368 \pm 0.024 \pm 0.007$	$0.42 \pm 0.04 \pm 0.01$	
$20 - 21$	$0.491 \pm 0.033 \pm 0.002$	$0.460 \pm 0.021 \pm 0.003$	$0.409 \pm 0.022 \pm 0.005$	$0.46 \pm 0.04 \pm 0.01$	
$21 - 22$					
$22 - 23$	$0.46 \pm 0.04 \pm 0.01$	$0.463 \pm 0.027 \pm 0.002$	$0.440 \pm 0.032 \pm 0.004$		
$23 - 24$					
$24 - 25$	$0.51 \pm 0.05 \pm 0.01$	$0.473 \pm 0.035 \pm 0.001$	$0.49 \pm 0.05 \pm 0.01$		
$25 - 26$					
$26 - 27$	$0.46 \pm 0.05 \pm 0.01$	$0.51 \pm 0.05 \pm 0.01$	$0.44 \pm 0.04 \pm 0.01$		
$27 - 28$					
$28 - 29$		$0.49 \pm 0.06 \pm 0.01$			
$29 - 30$					

Table 15: The ratio $\mathscr{R}_{3,1}$ for $\sqrt{s} = 8\,\text{TeV}$. The first uncertainties are statistical and the second are the uncorrelated component of the systematic uncertainties. The overall correlated systematic uncertainty is 0.7% and is not included in the numbers in the table. The horizontal lines indicate bin boundaries.

p_{T} [GeV/c]	$2.0 < y < 2.5$	$2.5 < y < 3.0$	$3.0 < y < 3.5$	$3.5 < y < 4.0$	$4.0 < y < 4.5$
$0 - 1$	$0.086 \pm 0.004 \pm 0.001$	$0.089 \pm 0.003 \pm 0.001$	$0.083 \pm 0.003 \pm 0.001$	$0.092 \pm 0.003 \pm 0.001$	$0.093 \pm 0.007 \pm 0.001$
$1 - 2$	$0.083 \pm 0.003 \pm 0.001$	$0.090 \pm 0.002 \pm 0.001$	$0.088 \pm 0.002 \pm 0.001$	$0.089 \pm 0.002 \pm 0.001$	$0.087 \pm 0.004 \pm 0.002$
$2 - 3$	$0.086 \pm 0.003 \pm 0.001$	$0.091 \pm 0.002 \pm 0.001$	$0.087 \pm 0.002 \pm 0.001$	$0.094 \pm 0.001 \pm 0.001$	$0.103 \pm 0.004 \pm 0.001$
$3 - 4$	$0.098 \pm 0.003 \pm 0.001$	$0.098 \pm 0.002 \pm 0.001$	$0.098 \pm 0.002 \pm 0.001$	$0.100 \pm 0.002 \pm 0.001$	$0.102 \pm 0.004 \pm 0.001$
$4 - 5$	$0.099 \pm 0.003 \pm 0.001$	$0.107 \pm 0.002 \pm 0.001$	$0.107 \pm 0.002 \pm 0.001$	$0.111 \pm 0.002 \pm 0.001$	$0.117 \pm 0.005 \pm 0.004$
$5 - 6$	$0.107 \pm 0.003 \pm 0.001$	$0.115 \pm 0.002 \pm 0.001$	$0.117 \pm 0.002 \pm 0.001$	$0.121 \pm 0.003 \pm 0.001$	$0.117 \pm 0.005 \pm 0.001$
$6 - 7$	$0.126 \pm 0.004 \pm 0.001$	$0.125 \pm 0.002 \pm 0.001$	$0.132 \pm 0.002 \pm 0.001$	$0.135 \pm 0.003 \pm 0.002$	$0.135 \pm 0.006 \pm 0.001$
$7 - 8$	$0.138 \pm 0.004 \pm 0.001$	$0.142 \pm 0.003 \pm 0.001$	$0.144 \pm 0.003 \pm 0.001$	$0.152 \pm 0.004 \pm 0.001$	$0.141 \pm 0.007 \pm 0.001$
$8 - 9$	$0.155 \pm 0.005 \pm 0.001$	$0.154 \pm 0.003 \pm 0.001$	$0.156 \pm 0.003 \pm 0.001$	$0.157 \pm 0.004 \pm 0.001$	$0.147 \pm 0.009 \pm 0.003$
$9 - 10$	$0.162 \pm 0.006 \pm 0.001$	$0.160 \pm 0.004 \pm 0.001$	$0.170 \pm 0.004 \pm 0.001$	$0.183 \pm 0.005 \pm 0.002$	$0.157 \pm 0.012 \pm 0.001$
$10 - 11$	$0.164 \pm 0.007 \pm 0.001$	$0.180 \pm 0.005 \pm 0.002$	$0.186 \pm 0.005 \pm 0.001$	$0.205 \pm 0.007 \pm 0.002$	$0.220 \pm 0.019 \pm 0.009$
$11 - 12$	$0.176 \pm 0.008 \pm 0.003$	$0.193 \pm 0.005 \pm 0.001$	$0.198 \pm 0.005 \pm 0.003$	$0.195 \pm 0.007 \pm 0.001$	$0.213 \pm 0.024 \pm 0.004$
$12 - 13$	$0.211 \pm 0.010 \pm 0.002$	$0.221 \pm 0.006 \pm 0.001$	$0.216 \pm 0.007 \pm 0.001$	$0.224 \pm 0.009 \pm 0.002$	$0.192 \pm 0.031 \pm 0.002$
$13 - 14$	$0.236 \pm 0.013 \pm 0.001$	$0.228 \pm 0.007 \pm 0.001$	$0.227 \pm 0.008 \pm 0.003$	$0.235 \pm 0.011 \pm 0.002$	$0.245 \pm 0.040 \pm 0.008$
$14 - 15$	$0.245 \pm 0.015 \pm 0.003$	$0.248 \pm 0.009 \pm 0.003$	$0.236 \pm 0.010 \pm 0.001$	$0.257 \pm 0.014 \pm 0.005$	
$15 - 16$	$0.258 \pm 0.017 \pm 0.002$	$0.236 \pm 0.010 \pm 0.002$	$0.248 \pm 0.011 \pm 0.002$	$0.271 \pm 0.017 \pm 0.001$	
$16 - 17$	$0.251 \pm 0.019 \pm 0.003$	$0.263 \pm 0.012 \pm 0.002$	$0.272 \pm 0.014 \pm 0.001$	$0.235 \pm 0.019 \pm 0.006$	
$17 - 18$	$0.265 \pm 0.022 \pm 0.002$	$0.274 \pm 0.014 \pm 0.001$	$0.283 \pm 0.017 \pm 0.001$	$0.322 \pm 0.028 \pm 0.002$	$0.263 \pm 0.050 \pm 0.002$
$18 - 19$	$0.283 \pm 0.024 \pm 0.002$	$0.277 \pm 0.017 \pm 0.002$	$0.278 \pm 0.018 \pm 0.001$	$0.343 \pm 0.035 \pm 0.004$	
$19 - 20$	$0.290 \pm 0.029 \pm 0.001$	$0.292 \pm 0.019 \pm 0.001$	$0.257 \pm 0.020 \pm 0.003$	$0.268 \pm 0.034 \pm 0.007$	
$20 - 21$	$0.310 \pm 0.025 \pm 0.002$	$0.312 \pm 0.017 \pm 0.004$	$0.273 \pm 0.018 \pm 0.005$		
$21 - 22$					
$22 - 23$	$0.308 \pm 0.032 \pm 0.002$	$0.334 \pm 0.023 \pm 0.001$	$0.348 \pm 0.028 \pm 0.002$	$0.355 \pm 0.032 \pm 0.009$	
$23 - 24$					
$24 - 25$	$0.275 \pm 0.035 \pm 0.001$	$0.353 \pm 0.029 \pm 0.002$	$0.374 \pm 0.040 \pm 0.002$		
$25 - 26$					
$26 - 27$	$0.430 \pm 0.050 \pm 0.005$	$0.325 \pm 0.040 \pm 0.001$	$0.329 \pm 0.040 \pm 0.005$		
$27 - 28$					
$28 - 29$		$0.310 \pm 0.040 \pm 0.004$			
$29 - 30$					

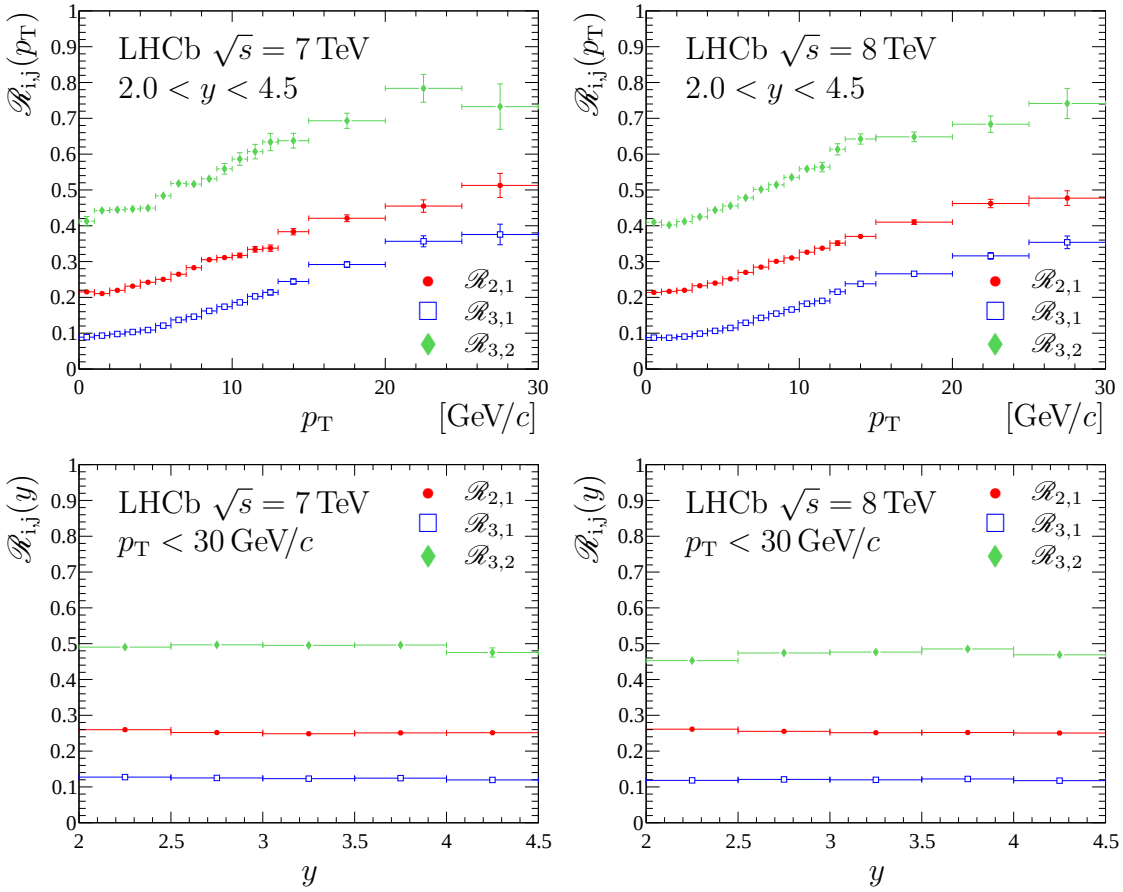

Figure 7: The production ratios (red solid circles) $\mathscr{R}_{2,1}$, (blue open squares) $\mathscr{R}_{3,1}$ and (green solid diamonds) $\mathscr{R}_{3,2}$ for (left) $\sqrt{s} = 7\,\text{TeV}$ and (right) $\sqrt{s} = 8\,\text{TeV}$ data, integrated over the (top) $2.0 < y < 4.5$ region and (bottom) $p_T < 30\,\text{GeV}/c$ region.

6 Summary

The forward production of Υ mesons is studied in pp collisions at centre-of-mass energies of 7 and 8 TeV using data samples corresponding to integrated luminosities of $1\,\text{fb}^{-1}$ and $2\,\text{fb}^{-1}$ respectively, collected with the LHCb detector. The double differential production cross-sections are measured as a function of meson transverse momenta and rapidity for the range $p_T < 30\,\text{GeV}/c$, $2.0 < y < 4.5$. The measured increase in the production cross-sections of Υ mesons between $\sqrt{s} = 8$ and 7 TeV significantly exceeds theory expectations and confirms the previous LHCb observations [22, 23]. For the region $p_T < 15\,\text{GeV}/c$ the results agree with the previous measurements [22, 23], and supersede them.

Table 16: The ratios $\mathscr{R}_{\rm i,j}$ in the full kinematic range $p_{\rm T} < 30\,{\rm GeV}/c$ and in the reduced range $p_{\rm T} < 15\,{\rm GeV}/c$ for $2.0 < y < 4.5$. The first uncertainties are statistical and the second systematic.

	$\sqrt{s} = 7\,{\rm TeV}$	$\sqrt{s} = 8\,{\rm TeV}$
	$p_{\rm T} < 30\,{\rm GeV}/c$	
$\mathscr{R}_{2,1}$	$0.253 \pm 0.001 \pm 0.004$	$0.255 \pm 0.001 \pm 0.004$
$\mathscr{R}_{3,1}$	$0.125 \pm 0.001 \pm 0.002$	$0.120 \pm 0.000 \pm 0.002$
$\mathscr{R}_{3,2}$	$0.493 \pm 0.003 \pm 0.007$	$0.470 \pm 0.002 \pm 0.007$
	$p_{\rm T} < 15\,{\rm GeV}/c$	
$\mathscr{R}_{2,1}$	$0.249 \pm 0.001 \pm 0.004$	$0.251 \pm 0.001 \pm 0.004$
$\mathscr{R}_{3,1}$	$0.121 \pm 0.001 \pm 0.002$	$0.116 \pm 0.000 \pm 0.002$
$\mathscr{R}_{3,2}$	$0.485 \pm 0.003 \pm 0.007$	$0.463 \pm 0.002 \pm 0.007$

Acknowledgements

We thank K.-T. Chao, H. Han and H.-S. Shao for providing the theory predictions for our measurements. We also would like to thank S. P. Baranov, L. S. Kisslinger, J.-P. Lansberg, A. K. Likhoded and A. V. Luchinsky for interesting and stimulating discussions on quarkonia production. We express our gratitude to our colleagues in the CERN accelerator departments for the excellent performance of the LHC. We thank the technical and administrative staff at the LHCb institutes. We acknowledge support from CERN and from the national agencies: CAPES, CNPq, FAPERJ and FINEP (Brazil); NSFC (China); CNRS/IN2P3 (France); BMBF, DFG, HGF and MPG (Germany); INFN (Italy); FOM and NWO (The Netherlands); MNiSW and NCN (Poland); MEN/IFA (Romania); MinES and FANO (Russia); MinECo (Spain); SNSF and SER (Switzerland); NASU (Ukraine); STFC (United Kingdom); NSF (USA). The Tier1 computing centres are supported by IN2P3 (France), KIT and BMBF (Germany), INFN (Italy), NWO and SURF (The Netherlands), PIC (Spain), GridPP (United Kingdom). We are indebted to the communities behind the multiple open source software packages on which we depend. We are also thankful for the computing resources and the access to software R&D tools provided by Yandex LLC (Russia). Individual groups or members have received support from EPLANET, Marie Skłodowska-Curie Actions and ERC (European Union), Conseil général de Haute-Savoie, Labex ENIGMASS and OCEVU, Région Auvergne (France), RFBR (Russia), XuntaGal and GENCAT (Spain), Royal Society and Royal Commission for the Exhibition of 1851 (United Kingdom).

References

[1] W. E. Caswell and G. P. Lepage, *Effective Lagrangians for bound state problems in QED, QCD, and other field theories*, Phys. Lett. **B167** (1986) 437.

[2] G. T. Bodwin, E. Braaten, and G. P. Lepage, *Rigorous QCD analysis of inclusive annihilation and production of heavy quarkonium*, Phys. Rev. **D51** (1995) 1125.

[3] V. G. Kartvelishvili, A. K. Likhoded, and S. R. Slabospitsky, D *meson and* ψ *meson production in hadronic interactions*, Sov. J. Nucl. Phys. **28** (1978) 678, [Yad. Fiz. **28** (1978) 1315].

[4] R. Baier and R. Rückl, *Hadronic production of* J/ψ *and* Υ*: transverse momentum distributions*, Phys. Lett. **B102** (1981) 364.

[5] CDF collaboration, F. Abe *et al.*, *Inclusive* J/ψ , ψ(2S) *and* b *quark production in* $\overline{\mathrm{p}}$p *collisions at* $\sqrt{s} = 1.8$ *TeV*, Phys. Rev. Lett. **69** (1992) 3704.

[6] E. Braaten and S. Fleming, *Color octet fragmentation and the* ψ' *surplus at the Tevatron*, Phys. Rev. Lett. **74** (1995) 3327, arXiv:hep-ph/9411365.

[7] J. M. Campbell, F. Maltoni, and F. Tramontano, *QCD corrections to* J/ψ *and* Υ *production at hadron colliders*, Phys. Rev. Lett. **98** (2007) 252002, arXiv:hep-ph/0703113.

[8] B. Gong and J.-X. Wang, *Next-to-leading-order QCD corrections to* J/ψ *polarization at Tevatron and Large-Hadron-Collider energies*, Phys. Rev. Lett. **100** (2008) 232001, arXiv:0802.3727.

[9] P. Artoisenet *et al.*, Υ *production at Fermilab Tevatron and LHC energies*, Phys. Rev. Lett. **101** (2008) 152001, arXiv:0806.3282.

[10] J.-P. Lansberg, *On the mechanisms of heavy-quarkonium hadroproduction*, Eur. Phy. J. **C61** (2008) 693, arXiv:0811.4005.

[11] H. Han *et al.*, Υ(nS) *and* χ_{b}(nP) *production at hadron colliders in nonrelativistic QCD*, arXiv:1410.8537.

[12] N. Brambilla *et al.*, *Heavy quarkonium: progress, puzzles, and opportunities*, Eur. Phys. J. **C71** (2011) 1534, arXiv:1010.5827.

[13] ATLAS collaboration, G. Aad *et al.*, *Observation of a new* χ_{b} *state in radiative transitions to* Υ(1S) *and* Υ(2S) *at ATLAS*, Phys. Rev. Lett. **108** (2012) 152001, arXiv:1112.5154.

[14] D0 collaboration, V. M. Abazov *et al.*, *Observation of a narrow mass state decaying into* $\Upsilon(1\mathrm{S}) + \gamma$ *in* $\mathrm{p\overline{p}}$ *collisions at* $\sqrt{s} = 1.96$ *TeV*, Phys. Rev. **D86** (2012) 031103, arXiv:1203.6034.

[15] LHCb collaboration, R. Aaij *et al.*, *Measurement of the fraction of* $\Upsilon(1S)$ *originating from* $\chi_b(1P)$ *decays in* pp *collisions at* $\sqrt{s} = 7\ TeV$, JHEP **11** (2012) 031, arXiv:1209.0282.

[16] LHCb collaboration, R. Aaij *et al.*, *Study of* χ_b *meson production in* pp *collisions at* $\sqrt{s} = 7$ *and* $8\ TeV$ *and observation of the decay* $\chi_b \to \Upsilon(3S)\gamma$, Eur. Phys. J. **C74** (2014) 3092, arXiv:1407.7734.

[17] A. Mazurov, *High Level Trigger software performance profiling and* χ_b *production study at the LHCb experiment*, PhD thesis, Ferrara University, Ferrara, 2014, CERN-THESIS-2014-016.

[18] LHCb collaboration, R. Aaij *et al.*, *Measurement of the* $\chi_b(3P)$ *mass and of the relative rate of* $\chi_{b1}(1P)$ *and* $\chi_{b2}(1P)$ *production*, JHEP **10** (2014) 088, arXiv:1409.1408.

[19] A. K. Likhoded, A. V. Luchinsky, and S. V. Poslavsky, *Production of* χ_b*-mesons at LHC*, Phys. Rev. **D86** (2012) 074027, arXiv:1203.4893.

[20] K. Wang, Y.-Q. Ma, and K.-T. Chao, $\Upsilon(1S)$ *prompt production at the Tevatron and LHC in nonrelativistic QCD*, Phys. Rev. **D85** (2012) 114003, arXiv:1202.6012.

[21] LHCb collaboration, R. Aaij *et al.*, *Measurement of* Υ *production in* pp *collisions at* $\sqrt{s} = 2.76\ TeV$, Eur. Phys. J. **C74** (2014) 2835, arXiv:1402.2539.

[22] LHCb collaboration, R. Aaij *et al.*, *Measurement of* Υ *production in* pp *collisions at* $\sqrt{s} = 7\ TeV$, Eur. Phys. J. **C72** (2012) 2025, arXiv:1202.6579.

[23] LHCb collaboration, R. Aaij *et al.*, *Production of* J/ψ *and* Υ *mesons in* pp *collisions at* $\sqrt{s} = 8\ TeV$, JHEP **06** (2013) 064, arXiv:1304.6977.

[24] ALICE collaboration, B. B. Abelev *et al.*, *Measurement of quarkonium production at forward rapidity in* pp *collisions at* $\sqrt{s} = 7\ TeV$, Eur. Phys. J. **C74** (2014) 2974, arXiv:1403.3648.

[25] ATLAS collaboration, G. Aad *et al.*, *Measurement of* Υ *production in* $7\ TeV$ pp *collisions at ATLAS*, Phys. Rev **D87** (2013) 052004, arXiv:1211.7255.

[26] CMS collaboration, V. Khachatryan *et al.*, Υ *production cross section in* pp *collisions at* $\sqrt{s} = 7\ TeV$, Phys. Rev. **D83** (2011) 112004, arXiv:1012.5545.

[27] CMS collaboration, S. Chatrchyan *et al.*, *Measurement of the* $\Upsilon(1S)$, $\Upsilon(2S)$, *and* $\Upsilon(3S)$ *cross sections in* pp *collisions at* $\sqrt{s} = 7\ TeV$, Phys. Lett. **B727** (2013) 101, arXiv:1303.5900.

[28] LHCb collaboration, R. Aaij *et al.*, *Measurement of* J/ψ *production in* pp *collisions at* $\sqrt{s} = 7\ TeV$, Eur. Phys. J. **C71** (2011) 1645, arXiv:1103.0423.

[29] LHCb collaboration, A. A. Alves Jr. *et al.*, *The LHCb detector at the LHC*, JINST **3** (2008) S08005.

[30] LHCb collaboration, R. Aaij *et al.*, *LHCb detector performance*, Int. J. Mod. Phys. **A30** (2015) 1530022, arXiv:1412.6352.

[31] A. A. Alves Jr. *et al.*, *Performance of the LHCb muon system*, JINST **8** (2013) P02022, arXiv:1211.1346.

[32] R. Aaij *et al.*, *The LHCb trigger and its performance in 2011*, JINST **8** (2013) P04022, arXiv:1211.3055.

[33] T. Sjöstrand, S. Mrenna, and P. Skands, PYTHIA *6.4 physics and manual*, JHEP **05** (2006) 026, arXiv:hep-ph/0603175.

[34] I. Belyaev *et al.*, *Handling of the generation of primary events in* GAUSS*, the LHCb simulation framework*, J. Phys. Conf. Ser. **331** (2011) 032047.

[35] D. J. Lange, *The* EVTGEN *particle decay simulation package*, Nucl. Instrum. Meth. **A462** (2001) 152.

[36] P. Golonka and Z. Was, PHOTOS *Monte Carlo: A precision tool for QED corrections in* Z *and* W *decays*, Eur. Phys. J. **C45** (2006) 97, arXiv:hep-ph/0506026.

[37] Geant4 collaboration, J. Allison *et al.*, GEANT4 *developments and applications*, IEEE Trans. Nucl. Sci. **53** (2006) 270; Geant4 collaboration, S. Agostinelli *et al.*, GEANT4*: A simulation toolkit*, Nucl. Instrum. Meth. **A506** (2003) 250.

[38] M. Clemencic *et al.*, *The LHCb simulation application,* GAUSS*: Design, evolution and experience*, J. Phys. Conf. Ser. **331** (2011) 032023.

[39] LHCb collaboration, R. Aaij *et al.*, *Measurement of the track reconstruction efficiency at LHCb*, JINST **10** (2015) P02007, arXiv:1408.1251.

[40] F. Archilli *et al.*, *Performance of the muon identification at LHCb*, JINST **8** (2013) P10020, arXiv:1306.0249.

[41] W. D. Hulsbergen, *Decay chain fitting with a Kalman filter*, Nucl. Instrum. Meth. **A552** (2005) 566, arXiv:physics/0503191.

[42] Particle Data Group, K. A. Olive *et al.*, *Review of particle physics*, Chin. Phys. **C38** (2014) 090001.

[43] T. Skwarnicki, *A study of the radiative cascade transitions between the* Υ' *and* Υ *resonances*, PhD thesis, Institute of Nuclear Physics, Krakow, 1986, DESY-F31-86-02.

[44] M. Pivk and F. R. Le Diberder, *sPlot: A statistical tool to unfold data distributions*, Nucl. Instrum. Meth. **A555** (2005) 356, arXiv:physics/0402083.

[45] S. van der Meer, *Calibration of the effective beam height in the ISR*, ISR-PO/68-31, 1968.

[46] M. Ferro-Luzzi, *Proposal for an absolute luminosity determination in colliding beam experiments using vertex detection of beam-gas interactions*, Nucl. Instrum. Meth. **A553** (2005) 388.

[47] LHCb collaboration, R. Aaij *et al.*, *Absolute luminosity measurements with the LHCb detector at the LHC*, JINST **7** (2012) P01010, arXiv:1110.2866.

[48] LHCb collaboration, R. Aaij *et al.*, *Precision luminosity measurements at LHCb*, JINST **9** (2014) P12005, arXiv:1410.0149.

[49] C. Barschel, *Precision luminosity measurement at LHCb with beam-gas imaging*, PhD thesis, RWTH Aachen, 2014, CERN-THESIS-2013-301.

[50] J. Wenninger, *Energy calibration of the LHC beams at* 4 TeV, Tech. Rep. CERN-ATS-2013-040, CERN, 2013.

[51] CMS collaboration, S. Chatrchyan *et al.*, *Measurement of the* Υ(1S), Υ(2S) *and* Υ(3S) *polarizations in* pp *collisions at* $\sqrt{s} = 7$ TeV, Phys. Rev. Lett. **110** (2013) 081802, arXiv:1209.2922.

[52] J. C. Collins and D. E. Soper, *Angular distribution of dileptons in high-energy hadron collisions*, Phys. Rev. **D16** (1977) 2219.

[53] C. Tsallis, *Possible generalization of Boltzmann-Gibbs statistic*, J. Statist. Phys. **52** (1988) 479.

[54] LHCb collaboration, R. Aaij *et al.*, *Study of differential productions of* Λ_b *and* $\bar{B}^0$ *hadrons in* pp *collisions and a measurement of the* $\Lambda_b \to J/\psi\, pK^-$ *branching fraction*, LHCb-PAPER-2015-032, in preparation.

[55] CMS collaboration, S. Chatrchyan *et al.*, *Measurement of the* Λ_b^0 *cross section and the* $\bar{\Lambda}_b$ *to* Λ_b^0 *ratio with* $\Lambda_b^0 \to J/\psi\,\Lambda$ *decays in* pp *collisions at* $\sqrt{s} = 7$ TeV, Phys. Lett. **B714** (2012) 136, arXiv:1205.0594.

[56] H. Zheng, L. Zhu, and A. Bonasera, *Systematic analysis of hadron spectra in* pp *collisions using Tsallis distribution*, arXiv:1506.03156.

[57] L. Marques, J. Cleymans, and A. Deppman, *Description of high-energy* pp *collisions using Tsallis thermodynamics: transverse momentum and rapidity distributions*, Phys. Rev. **D91** (2015) 054025, arXiv:1501.00953.

[58] E. L. Berger and D. Jones, *Inelastic photoproduction of* J/ψ *and* Υ *by gluons*, Phys. Rev. **D23** (1981) 1521.

[59] C.-H. Chang, *Hadronic production of* J/ψ *associated with a gluon*, Nucl. Phys. **B172** (1980) 425.

[60] R. Baier and R. Rückl, *Hadronic collisions: a quarkonium factory*, Z. Phys. **C19** (1983) 251.

[61] G. D. Lafferty and T. R. Wyatt, *Where to stick your data points: the treatment of measurements within wide bins*, Nucl. Instrum. Meth. **A355** (1995) 541.

[62] L. S. Kisslinger, M. X. Liu, and P. McGaughey, *Heavy quark state production in* pp *collisions*, Phys. Rev. **D84** (2011) 114020, Erratum ibid. **D86** (2012) 039902, arXiv:1108.4049.

[63] L. S. Kisslinger and D. Das, Ψ *and* Υ *production in* pp *collisions at* 7.0 TeV, Mod. Phys. Lett. **A28** (2013) 1350120, arXiv:1306.6616; L. S. Kisslinger and D. Das, Ψ *and* Υ *production in* pp *collisions at* 8.0 TeV, Mod. Phys. Lett. **A29** (2014) 1450082, arXiv:1403.2271.

[64] M. Cacciari, M. Greco, and P. Nason, *The* $p_{\rm T}$ *spectrum in heavy flavor hadroproduction*, JHEP **05** (1998) 007, arXiv:hep-ph/9803400; M. Cacciari, S. Frixione, and P. Nason, *The* $p_{\rm T}$ *spectrum in heavy flavor photoproduction*, JHEP **03** (2001) 006, arXiv:hep-ph/0102134; M. Cacciari *et al.*, *Theoretical predictions for charm and bottom production at the LHC*, JHEP **10** (2012) 137, arXiv:1205.6344.

[65] L. S. Kisslinger, *Mixed heavy quark hybrid mesons, decay puzzles, and RHIC*, Phys. Rev. **D79** (2009) 114026, arXiv:0903.1120; L. S. Kisslinger and D. Das, *Upsilon production in* pp *collisions for forward rapidities at LHC*, Mod. Phys. Lett. **A28** (2013) 1350067, arXiv:1207.3296; L. S. Kisslinger, *Upsilon production in* pp *collisions at LHC*, Mod. Phys. Lett. **A27** (2012) 1250074, arXiv:1201.1033.

LHCb collaboration

R. Aaij[38], B. Adeva[37], M. Adinolfi[46], A. Affolder[52], Z. Ajaltouni[5], S. Akar[6], J. Albrecht[9], F. Alessio[38], M. Alexander[51], S. Ali[41], G. Alkhazov[30], P. Alvarez Cartelle[53], A.A. Alves Jr[57], S. Amato[2], S. Amerio[22], Y. Amhis[7], L. An[3], L. Anderlini[17], J. Anderson[40], G. Andreassi[39], M. Andreotti[16,f], J.E. Andrews[58], R.B. Appleby[54], O. Aquines Gutierrez[10], F. Archilli[38], P. d'Argent[11], A. Artamonov[35], M. Artuso[59], E. Aslanides[6], G. Auriemma[25,m], M. Baalouch[5], S. Bachmann[11], J.J. Back[48], A. Badalov[36], C. Baesso[60], W. Baldini[16,38], R.J. Barlow[54], C. Barschel[38], S. Barsuk[7], W. Barter[38], V. Batozskaya[28], V. Battista[39], A. Bay[39], L. Beaucourt[4], J. Beddow[51], F. Bedeschi[23], I. Bediaga[1], L.J. Bel[41], V. Bellee[39], N. Belloli[20,j], I. Belyaev[31], E. Ben-Haim[8], G. Bencivenni[18], S. Benson[38], J. Benton[46], A. Berezhnoy[32], R. Bernet[40], A. Bertolin[22], M.-O. Bettler[38], M. van Beuzekom[41], A. Bien[11], S. Bifani[45], P. Billoir[8], T. Bird[54], A. Birnkraut[9], A. Bizzeti[17,h], T. Blake[48], F. Blanc[39], J. Blouw[10], S. Blusk[59], V. Bocci[25], A. Bondar[34], N. Bondar[30,38], W. Bonivento[15], S. Borghi[54], M. Borsato[7], T.J.V. Bowcock[52], E. Bowen[40], C. Bozzi[16], S. Braun[11], M. Britsch[10], T. Britton[59], J. Brodzicka[54], N.H. Brook[46], E. Buchanan[46], A. Bursche[40], J. Buytaert[38], S. Cadeddu[15], R. Calabrese[16,f], M. Calvi[20,j], M. Calvo Gomez[36,o], P. Campana[18], D. Campora Perez[38], L. Capriotti[54], A. Carbone[14,d], G. Carboni[24,k], R. Cardinale[19,i], A. Cardini[15], P. Carniti[20,j], L. Carson[50], K. Carvalho Akiba[2,38], G. Casse[52], L. Cassina[20,j], L. Castillo Garcia[38], M. Cattaneo[38], Ch. Cauet[9], G. Cavallero[19], R. Cenci[23,s], M. Charles[8], Ph. Charpentier[38], M. Chefdeville[4], S. Chen[54], S.-F. Cheung[55], N. Chiapolini[40], M. Chrzaszcz[40], X. Cid Vidal[38], G. Ciezarek[41], P.E.L. Clarke[50], M. Clemencic[38], H.V. Cliff[47], J. Closier[38], V. Coco[38], J. Cogan[6], E. Cogneras[5], V. Cogoni[15,e], L. Cojocariu[29], G. Collazuol[22], P. Collins[38], A. Comerma-Montells[11], A. Contu[15], A. Cook[46], M. Coombes[46], S. Coquereau[8], G. Corti[38], M. Corvo[16,f], B. Couturier[38], G.A. Cowan[50], D.C. Craik[48], A. Crocombe[48], M. Cruz Torres[60], S. Cunliffe[53], R. Currie[53], C. D'Ambrosio[38], E. Dall'Occo[41], J. Dalseno[46], P.N.Y. David[41], A. Davis[57], K. De Bruyn[6], S. De Capua[54], M. De Cian[11], J.M. De Miranda[1], L. De Paula[2], P. De Simone[18], C.-T. Dean[51], D. Decamp[4], M. Deckenhoff[9], L. Del Buono[8], N. Déléage[4], M. Demmer[9], D. Derkach[65], O. Deschamps[5], F. Dettori[38], B. Dey[21], A. Di Canto[38], F. Di Ruscio[24], H. Dijkstra[38], S. Donleavy[52], F. Dordei[11], M. Dorigo[39], A. Dosil Suárez[37], D. Dossett[48], A. Dovbnya[43], K. Dreimanis[52], L. Dufour[41], G. Dujany[54], P. Durante[38], R. Dzhelyadin[35], A. Dziurda[26], A. Dzyuba[30], S. Easo[49,38], U. Egede[53], V. Egorychev[31], S. Eidelman[34], S. Eisenhardt[50], U. Eitschberger[9], R. Ekelhof[9], L. Eklund[51], I. El Rifai[5], Ch. Elsasser[40], S. Ely[59], S. Esen[11], H.M. Evans[47], T. Evans[55], A. Falabella[14], C. Färber[38], N. Farley[45], S. Farry[52], R. Fay[52], D. Ferguson[50], V. Fernandez Albor[37], F. Ferrari[14], F. Ferreira Rodrigues[1], M. Ferro-Luzzi[38], S. Filippov[33], M. Fiore[16,38,f], M. Fiorini[16,f], M. Firlej[27], C. Fitzpatrick[39], T. Fiutowski[27], K. Fohl[38], P. Fol[53], M. Fontana[15], F. Fontanelli[19,i], R. Forty[38], O. Francisco[2], M. Frank[38], C. Frei[38], M. Frosini[17], J. Fu[21], E. Furfaro[24,k], A. Gallas Torreira[37], D. Galli[14,d], S. Gallorini[22], S. Gambetta[50], M. Gandelman[2], P. Gandini[55], Y. Gao[3], J. García Pardiñas[37], J. Garra Tico[47], L. Garrido[36], D. Gascon[36], C. Gaspar[38], R. Gauld[55], L. Gavardi[9], G. Gazzoni[5], D. Gerick[11], E. Gersabeck[11], M. Gersabeck[54], T. Gershon[48], Ph. Ghez[4], S. Gianì[39], V. Gibson[47], O.G. Girard[39], L. Giubega[29], V.V. Gligorov[38], C. Göbel[60], D. Golubkov[31], A. Golutvin[53,38], A. Gomes[1,a], C. Gotti[20,j], M. Grabalosa Gándara[5], R. Graciani Diaz[36], L.A. Granado Cardoso[38], E. Graugés[36], E. Graverini[40], G. Graziani[17], A. Grecu[29], E. Greening[55], S. Gregson[47], P. Griffith[45], L. Grillo[11], O. Grünberg[63], B. Gui[59], E. Gushchin[33], Yu. Guz[35,38], T. Gys[38], T. Hadavizadeh[55], C. Hadjivasiliou[59], G. Haefeli[39], C. Haen[38], S.C. Haines[47], S. Hall[53], B. Hamilton[58], X. Han[11], S. Hansmann-Menzemer[11],

N. Harnew[55], S.T. Harnew[46], J. Harrison[54], J. He[38], T. Head[39], V. Heijne[41], K. Hennessy[52], P. Henrard[5], L. Henry[8], E. van Herwijnen[38], M. Heß[63], A. Hicheur[2], D. Hill[55], M. Hoballah[5], C. Hombach[54], W. Hulsbergen[41], T. Humair[53], N. Hussain[55], D. Hutchcroft[52], D. Hynds[51], M. Idzik[27], P. Ilten[56], R. Jacobsson[38], A. Jaeger[11], J. Jalocha[55], E. Jans[41], A. Jawahery[58], M. John[55], D. Johnson[38], C.R. Jones[47], C. Joram[38], B. Jost[38], N. Jurik[59], S. Kandybei[43], W. Kanso[6], M. Karacson[38], T.M. Karbach[38,†], S. Karodia[51], M. Kecke[11], M. Kelsey[59], I.R. Kenyon[45], M. Kenzie[38], T. Ketel[42], E. Khairullin[65], B. Khanji[20,38,j], C. Khurewathanakul[39], S. Klaver[54], K. Klimaszewski[28], O. Kochebina[7], M. Kolpin[11], I. Komarov[39], R.F. Koopman[42], P. Koppenburg[41,38], M. Kozeiha[5], L. Kravchuk[33], K. Kreplin[11], M. Kreps[48], G. Krocker[11], P. Krokovny[34], F. Kruse[9], W. Krzemien[28], W. Kucewicz[26,n], M. Kucharczyk[26], V. Kudryavtsev[34], A. K. Kuonen[39], K. Kurek[28], T. Kvaratskheliya[31], D. Lacarrere[38], G. Lafferty[54], A. Lai[15], D. Lambert[50], G. Lanfranchi[18], C. Langenbruch[48], B. Langhans[38], T. Latham[48], C. Lazzeroni[45], R. Le Gac[6], J. van Leerdam[41], J.-P. Lees[4], R. Lefèvre[5], A. Leflat[32,38], J. Lefrançois[7], E. Lemos Cid[37], O. Leroy[6], T. Lesiak[26], B. Leverington[11], Y. Li[7], T. Likhomanenko[65,64], M. Liles[52], R. Lindner[38], C. Linn[38], F. Lionetto[40], B. Liu[15], X. Liu[3], D. Loh[48], I. Longstaff[51], J.H. Lopes[2], D. Lucchesi[22,q], M. Lucio Martinez[37], H. Luo[50], A. Lupato[22], E. Luppi[16,f], O. Lupton[55], A. Lusiani[23], F. Machefert[7], F. Maciuc[29], O. Maev[30], K. Maguire[54], S. Malde[55], A. Malinin[64], G. Manca[7], G. Mancinelli[6], P. Manning[59], A. Mapelli[38], J. Maratas[5], J.F. Marchand[4], U. Marconi[14], C. Marin Benito[36], P. Marino[23,38,s], J. Marks[11], G. Martellotti[25], M. Martin[6], M. Martinelli[39], D. Martinez Santos[37], F. Martinez Vidal[66], D. Martins Tostes[2], A. Massafferri[1], R. Matev[38], A. Mathad[48], Z. Mathe[38], C. Matteuzzi[20], A. Mauri[40], B. Maurin[39], A. Mazurov[45], M. McCann[53], J. McCarthy[45], A. McNab[54], R. McNulty[12], B. Meadows[57], F. Meier[9], M. Meissner[11], D. Melnychuk[28], M. Merk[41], E Michielin[22], D.A. Milanes[62], M.-N. Minard[4], D.S. Mitzel[11], J. Molina Rodriguez[60], I.A. Monroy[62], S. Monteil[5], M. Morandin[22], P. Morawski[27], A. Mordà[6], M.J. Morello[23,s], J. Moron[27], A.B. Morris[50], R. Mountain[59], F. Muheim[50], D. Müller[54], J. Müller[9], K. Müller[40], V. Müller[9], M. Mussini[14], B. Muster[39], P. Naik[46], T. Nakada[39], R. Nandakumar[49], A. Nandi[55], I. Nasteva[2], M. Needham[50], N. Neri[21], S. Neubert[11], N. Neufeld[38], M. Neuner[11], A.D. Nguyen[39], T.D. Nguyen[39], C. Nguyen-Mau[39,p], V. Niess[5], R. Niet[9], N. Nikitin[32], T. Nikodem[11], A. Novoselov[35], D.P. O'Hanlon[48], A. Oblakowska-Mucha[27], V. Obraztsov[35], S. Ogilvy[51], O. Okhrimenko[44], R. Oldeman[15,e], C.J.G. Onderwater[67], B. Osorio Rodrigues[1], J.M. Otalora Goicochea[2], A. Otto[38], P. Owen[53], A. Oyanguren[66], A. Palano[13,c], F. Palombo[21,t], M. Palutan[18], J. Panman[38], A. Papanestis[49], M. Pappagallo[51], L.L. Pappalardo[16,f], C. Pappenheimer[57], W. Parker[58], C. Parkes[54], G. Passaleva[17], G.D. Patel[52], M. Patel[53], C. Patrignani[19,i], A. Pearce[54,49], A. Pellegrino[41], G. Penso[25,l], M. Pepe Altarelli[38], S. Perazzini[14,d], P. Perret[5], L. Pescatore[45], K. Petridis[46], A. Petrolini[19,i], M. Petruzzo[21], E. Picatoste Olloqui[36], B. Pietrzyk[4], T. Pilař[48], D. Pinci[25], A. Pistone[19], A. Piucci[11], S. Playfer[50], M. Plo Casasus[37], T. Poikela[38], F. Polci[8], A. Poluektov[48,34], I. Polyakov[31], E. Polycarpo[2], A. Popov[35], D. Popov[10,38], B. Popovici[29], C. Potterat[2], E. Price[46], J.D. Price[52], J. Prisciandaro[37], A. Pritchard[52], C. Prouve[46], V. Pugatch[44], A. Puig Navarro[39], G. Punzi[23,r], W. Qian[4], R. Quagliani[7,46], B. Rachwal[26], J.H. Rademacker[46], M. Rama[23], M. Ramos Pernas[37], M.S. Rangel[2], I. Raniuk[43], N. Rauschmayr[38], G. Raven[42], F. Redi[53], S. Reichert[54], M.M. Reid[48], A.C. dos Reis[1], S. Ricciardi[49], S. Richards[46], M. Rihl[38], K. Rinnert[52], V. Rives Molina[36], P. Robbe[7,38], A.B. Rodrigues[1], E. Rodrigues[54], J.A. Rodriguez Lopez[62], P. Rodriguez Perez[54], S. Roiser[38], V. Romanovsky[35], A. Romero Vidal[37], J. W. Ronayne[12], M. Rotondo[22], T. Ruf[38], P. Ruiz Valls[66], J.J. Saborido Silva[37], N. Sagidova[30], P. Sail[51], B. Saitta[15,e],

V. Salustino Guimaraes[2], C. Sanchez Mayordomo[66], B. Sanmartin Sedes[37], R. Santacesaria[25], C. Santamarina Rios[37], M. Santimaria[18], E. Santovetti[24,k], A. Sarti[18,l], C. Satriano[25,m], A. Satta[24], D.M. Saunders[46], D. Savrina[31,32], M. Schiller[38], H. Schindler[38], M. Schlupp[9], M. Schmelling[10], T. Schmelzer[9], B. Schmidt[38], O. Schneider[39], A. Schopper[38], M. Schubiger[39], M.-H. Schune[7], R. Schwemmer[38], B. Sciascia[18], A. Sciubba[25,l], A. Semennikov[31], N. Serra[40], J. Serrano[6], L. Sestini[22], P. Seyfert[20], M. Shapkin[35], I. Shapoval[16,43,f], Y. Shcheglov[30], T. Shears[52], L. Shekhtman[34], V. Shevchenko[64], A. Shires[9], B.G. Siddi[16], R. Silva Coutinho[48,40], L. Silva de Oliveira[2], G. Simi[22], M. Sirendi[47], N. Skidmore[46], T. Skwarnicki[59], E. Smith[55,49], E. Smith[53], I.T. Smith[50], J. Smith[47], M. Smith[54], H. Snoek[41], M.D. Sokoloff[57,38], F.J.P. Soler[51], F. Soomro[39], D. Souza[46], B. Souza De Paula[2], B. Spaan[9], P. Spradlin[51], S. Sridharan[38], F. Stagni[38], M. Stahl[11], S. Stahl[38], S. Stefkova[53], O. Steinkamp[40], O. Stenyakin[35], S. Stevenson[55], S. Stoica[29], S. Stone[59], B. Storaci[40], S. Stracka[23,s], M. Straticiuc[29], U. Straumann[40], L. Sun[57], W. Sutcliffe[53], K. Swientek[27], S. Swientek[9], V. Syropoulos[42], M. Szczekowski[28], T. Szumlak[27], S. T'Jampens[4], A. Tayduganov[6], T. Tekampe[9], M. Teklishyn[7], G. Tellarini[16,f], F. Teubert[38], C. Thomas[55], E. Thomas[38], J. van Tilburg[41], V. Tisserand[4], M. Tobin[39], J. Todd[57], S. Tolk[42], L. Tomassetti[16,f], D. Tonelli[38], S. Topp-Joergensen[55], N. Torr[55], E. Tournefier[4], S. Tourneur[39], K. Trabelsi[39], M.T. Tran[39], M. Tresch[40], A. Trisovic[38], A. Tsaregorodtsev[6], P. Tsopelas[41], N. Tuning[41,38], A. Ukleja[28], A. Ustyuzhanin[65,64], U. Uwer[11], C. Vacca[15,e], V. Vagnoni[14], G. Valenti[14], A. Vallier[7], R. Vazquez Gomez[18], P. Vazquez Regueiro[37], C. Vázquez Sierra[37], S. Vecchi[16], J.J. Velthuis[46], M. Veltri[17,g], G. Veneziano[39], M. Vesterinen[11], B. Viaud[7], D. Vieira[2], M. Vieites Diaz[37], X. Vilasis-Cardona[36,o], V. Volkov[32], A. Vollhardt[40], D. Volyanskyy[10], D. Voong[46], A. Vorobyev[30], V. Vorobyev[34], C. Voß[63], J.A. de Vries[41], R. Waldi[63], C. Wallace[48], R. Wallace[12], J. Walsh[23], S. Wandernoth[11], J. Wang[59], D.R. Ward[47], N.K. Watson[45], D. Websdale[53], A. Weiden[40], M. Whitehead[48], G. Wilkinson[55,38], M. Wilkinson[59], M. Williams[38], M.P. Williams[45], M. Williams[56], T. Williams[45], F.F. Wilson[49], J. Wimberley[58], J. Wishahi[9], W. Wislicki[28], M. Witek[26], G. Wormser[7], S.A. Wotton[47], S. Wright[47], K. Wyllie[38], Y. Xie[61], Z. Xu[39], Z. Yang[3], J. Yu[61], X. Yuan[34], O. Yushchenko[35], M. Zangoli[14], M. Zavertyaev[10,b], L. Zhang[3], Y. Zhang[3], A. Zhelezov[11], A. Zhokhov[31], L. Zhong[3], S. Zucchelli[14].

[1] *Centro Brasileiro de Pesquisas Físicas (CBPF), Rio de Janeiro, Brazil*
[2] *Universidade Federal do Rio de Janeiro (UFRJ), Rio de Janeiro, Brazil*
[3] *Center for High Energy Physics, Tsinghua University, Beijing, China*
[4] *LAPP, Université Savoie Mont-Blanc, CNRS/IN2P3, Annecy-Le-Vieux, France*
[5] *Clermont Université, Université Blaise Pascal, CNRS/IN2P3, LPC, Clermont-Ferrand, France*
[6] *CPPM, Aix-Marseille Université, CNRS/IN2P3, Marseille, France*
[7] *LAL, Université Paris-Sud, CNRS/IN2P3, Orsay, France*
[8] *LPNHE, Université Pierre et Marie Curie, Université Paris Diderot, CNRS/IN2P3, Paris, France*
[9] *Fakultät Physik, Technische Universität Dortmund, Dortmund, Germany*
[10] *Max-Planck-Institut für Kernphysik (MPIK), Heidelberg, Germany*
[11] *Physikalisches Institut, Ruprecht-Karls-Universität Heidelberg, Heidelberg, Germany*
[12] *School of Physics, University College Dublin, Dublin, Ireland*
[13] *Sezione INFN di Bari, Bari, Italy*
[14] *Sezione INFN di Bologna, Bologna, Italy*
[15] *Sezione INFN di Cagliari, Cagliari, Italy*
[16] *Sezione INFN di Ferrara, Ferrara, Italy*
[17] *Sezione INFN di Firenze, Firenze, Italy*
[18] *Laboratori Nazionali dell'INFN di Frascati, Frascati, Italy*

[19] *Sezione INFN di Genova, Genova, Italy*
[20] *Sezione INFN di Milano Bicocca, Milano, Italy*
[21] *Sezione INFN di Milano, Milano, Italy*
[22] *Sezione INFN di Padova, Padova, Italy*
[23] *Sezione INFN di Pisa, Pisa, Italy*
[24] *Sezione INFN di Roma Tor Vergata, Roma, Italy*
[25] *Sezione INFN di Roma La Sapienza, Roma, Italy*
[26] *Henryk Niewodniczanski Institute of Nuclear Physics Polish Academy of Sciences, Kraków, Poland*
[27] *AGH - University of Science and Technology, Faculty of Physics and Applied Computer Science, Kraków, Poland*
[28] *National Center for Nuclear Research (NCBJ), Warsaw, Poland*
[29] *Horia Hulubei National Institute of Physics and Nuclear Engineering, Bucharest-Magurele, Romania*
[30] *Petersburg Nuclear Physics Institute (PNPI), Gatchina, Russia*
[31] *Institute of Theoretical and Experimental Physics (ITEP), Moscow, Russia*
[32] *Institute of Nuclear Physics, Moscow State University (SINP MSU), Moscow, Russia*
[33] *Institute for Nuclear Research of the Russian Academy of Sciences (INR RAN), Moscow, Russia*
[34] *Budker Institute of Nuclear Physics (SB RAS) and Novosibirsk State University, Novosibirsk, Russia*
[35] *Institute for High Energy Physics (IHEP), Protvino, Russia*
[36] *Universitat de Barcelona, Barcelona, Spain*
[37] *Universidad de Santiago de Compostela, Santiago de Compostela, Spain*
[38] *European Organization for Nuclear Research (CERN), Geneva, Switzerland*
[39] *Ecole Polytechnique Fédérale de Lausanne (EPFL), Lausanne, Switzerland*
[40] *Physik-Institut, Universität Zürich, Zürich, Switzerland*
[41] *Nikhef National Institute for Subatomic Physics, Amsterdam, The Netherlands*
[42] *Nikhef National Institute for Subatomic Physics and VU University Amsterdam, Amsterdam, The Netherlands*
[43] *NSC Kharkiv Institute of Physics and Technology (NSC KIPT), Kharkiv, Ukraine*
[44] *Institute for Nuclear Research of the National Academy of Sciences (KINR), Kyiv, Ukraine*
[45] *University of Birmingham, Birmingham, United Kingdom*
[46] *H.H. Wills Physics Laboratory, University of Bristol, Bristol, United Kingdom*
[47] *Cavendish Laboratory, University of Cambridge, Cambridge, United Kingdom*
[48] *Department of Physics, University of Warwick, Coventry, United Kingdom*
[49] *STFC Rutherford Appleton Laboratory, Didcot, United Kingdom*
[50] *School of Physics and Astronomy, University of Edinburgh, Edinburgh, United Kingdom*
[51] *School of Physics and Astronomy, University of Glasgow, Glasgow, United Kingdom*
[52] *Oliver Lodge Laboratory, University of Liverpool, Liverpool, United Kingdom*
[53] *Imperial College London, London, United Kingdom*
[54] *School of Physics and Astronomy, University of Manchester, Manchester, United Kingdom*
[55] *Department of Physics, University of Oxford, Oxford, United Kingdom*
[56] *Massachusetts Institute of Technology, Cambridge, MA, United States*
[57] *University of Cincinnati, Cincinnati, OH, United States*
[58] *University of Maryland, College Park, MD, United States*
[59] *Syracuse University, Syracuse, NY, United States*
[60] *Pontifícia Universidade Católica do Rio de Janeiro (PUC-Rio), Rio de Janeiro, Brazil, associated to* [2]
[61] *Institute of Particle Physics, Central China Normal University, Wuhan, Hubei, China, associated to* [3]
[62] *Departamento de Fisica , Universidad Nacional de Colombia, Bogota, Colombia, associated to* [8]
[63] *Institut für Physik, Universität Rostock, Rostock, Germany, associated to* [11]
[64] *National Research Centre Kurchatov Institute, Moscow, Russia, associated to* [31]
[65] *Yandex School of Data Analysis, Moscow, Russia, associated to* [31]
[66] *Instituto de Fisica Corpuscular (IFIC), Universitat de Valencia-CSIC, Valencia, Spain, associated to* [36]
[67] *Van Swinderen Institute, University of Groningen, Groningen, The Netherlands, associated to* [41]

[a] *Universidade Federal do Triângulo Mineiro (UFTM), Uberaba-MG, Brazil*
[b] *P.N. Lebedev Physical Institute, Russian Academy of Science (LPI RAS), Moscow, Russia*
[c] *Università di Bari, Bari, Italy*
[d] *Università di Bologna, Bologna, Italy*
[e] *Università di Cagliari, Cagliari, Italy*
[f] *Università di Ferrara, Ferrara, Italy*
[g] *Università di Urbino, Urbino, Italy*
[h] *Università di Modena e Reggio Emilia, Modena, Italy*
[i] *Università di Genova, Genova, Italy*
[j] *Università di Milano Bicocca, Milano, Italy*
[k] *Università di Roma Tor Vergata, Roma, Italy*
[l] *Università di Roma La Sapienza, Roma, Italy*
[m] *Università della Basilicata, Potenza, Italy*
[n] *AGH - University of Science and Technology, Faculty of Computer Science, Electronics and Telecommunications, Kraków, Poland*
[o] *LIFAELS, La Salle, Universitat Ramon Llull, Barcelona, Spain*
[p] *Hanoi University of Science, Hanoi, Viet Nam*
[q] *Università di Padova, Padova, Italy*
[r] *Università di Pisa, Pisa, Italy*
[s] *Scuola Normale Superiore, Pisa, Italy*
[t] *Università degli Studi di Milano, Milano, Italy*

[†] *Deceased*